Received ; | Revised ; | Accepted

DOI: xxx/xxxx

RESEARCH ARTICLE

Stability of an explicit high-order spectral element method for acoustics in heterogeneous media based on local element stability criteria

Régis Cottereau*[1] | Ruben Sevilla[2]

[1]Laboratoire MSSMat, CNRS, CentraleSupélec, Université Paris-Saclay, France

[2]Zienkiewicz Centre for Computational Engineering, College of Engineering, Swansea University, Wales, UK

Correspondence
*Régis Cottereau. Email: regis.cottereau@centralesupelec.fr

Summary

This paper considers the stability of an explicit Leap-Frog time marching scheme for the simulation of acoustic wave propagation in heterogeneous media with high-order spectral elements. The global stability criterion is taken as a minimum over local element stability criteria, obtained through the solution of element-borne eigenvalue problems. First, an explicit stability criterion is obtained for the particular case of a strongly-heterogeneous and/or rapidly-fluctuating medium using asymptotic analysis. This criterion is only dependent upon the maximum velocity at the vertices of the mesh elements, and not on the velocity at the interior nodes of the high-order elements. Second, in a more general setting, bounds are derived using statistics of the coefficients of the elemental dispersion matrices. Different bounds are presented, discussed and compared. Several numerical experiments show the accuracy of the proposed criteria in one-dimensional test cases as well as in more realistic large scale 3D problems.

KEYWORDS:
spectral element method, explicit time integration, stability, heterogeneous media, high-order

1 | INTRODUCTION

The numerical simulation of wave propagation phenomena is of great interest in many areas of science and engineering, including seismic [1], acoustic [2] and electromagnetic [3,4] applications. In this context, the use of time-domain solvers enables to significantly reduce the memory requirements and the need to devise effective preconditioners, when compared to frequency domain solvers. The efficiency of a time-domain simulation using explicit time marching algorithms is directly linked to the stability limit of the selected time marching scheme.

For a homogeneous one-dimensional problem with constant element size, the stability criterion for the spectral element method (SEM) is given by [5]

$$\alpha = \frac{c\Delta t}{h} \leq \alpha_M, \tag{1}$$

where c is the wave velocity, Δt is the time step and h is the characteristic element size. The stability limit, α_M, is a scalar that depends upon the polynomial order p. Its value can be derived analytically for homogeneous media [5,6,7,8,9]. Table 1 summarises the values for polynomial approximations up to order $p = 5$ when the SEM is combined with the Leap-Frog time marching scheme. For regular meshes in $\mathtt{n_{sd}}$ spatial dimensions, the value of the stability limit is simply that for one-dimensional problems divided by $\sqrt{\mathtt{n_{sd}}}$.

TABLE 1 Approximate value of the stability limit α_M for spectral elements of polynomial order p in d dimensions with the Leap-Frog scheme assuming a regular mesh and constant wave velocity.

n_{sd}	p=1	p=2	p=3	p=4	p=5
1	1.00	0.40	0.23	0.14	0.10
2	0.70	0.28	0.16	0.10	0.07
3	0.57	0.23	0.13	0.08	0.05

The results in Table 1 are derived for homogeneous material parameters and regular meshes. Numerical tests showing the negative influence of the deformation of quadrilateral elements on the stability are reported in [5,10,11]. For simplicial elements, the influence of distortion is analysed rigorously in [12] and for linear triangles and bi-linear quadrilaterals in [13]. Some hints can also be found about the error induced by the presence of a discontinuity or heterogeneity of the material properties [14,15,16,5], but general stability criteria have only been derived for specific finite-difference schemes [17]. When extrapolating the homogeneous stability criteria to heterogeneous media, the risk is either to run into unstable simulations by overestimating the stability limit or to waste computational resources by underestimating the stability limit.

In a previous paper [18], a classical Von Neumann stability analysis was proposed for the one-dimensional SEM with the Leap-Frog time integrator scheme in heterogeneous media with periodically-fluctuating material properties. Explicit stability criteria were derived for quadratic and cubic one-dimensional spectral elements when the periodicity of the fluctuating material properties was linked to the mesh element size. The analysis revealed the origin of instabilities that are often observed when the stability limit derived for homogeneous materials is adapted by simply using the lowest local velocity in Eq. (1). The main limitation of the analysis presented in [18] is the link between the periodicity of the material properties and the element size of the mesh, which precludes its application to a large class of problems, including those where the mechanical properties are modelled as realisations of random fields [19,20,21,22,23].

The objective of this work is to obtain a stability criterion that is accurate for a general heterogeneous medium. The strategy follows a methodology commonly employed in a finite element context (or by other element based methods) that consists of bounding the eigenvalues of a global matrix by the eigenvalues of the elemental matrices (Irons and Treharne theorem) [24]. On the one hand, this allows to bypass the hypothesis about periodic material properties used in [18], and on the other hand, it reformulates the global stability as a bounding problem on the maximum eigenvalue of certain local matrices. To obtain a stability criterion that is easier to compute in large scale implementations of explicit solvers, the maximum elemental eigenvalues are bounded using different approaches. The eigenvalue bounds are computed numerically and their accuracy and efficiency is analysed. In the particular situation of strongly-heterogeneous and/or rapidly-fluctuating material properties, an analytical approach to compute the stability criterion is also proposed. Although this bound is less accurate and general (not valid for slowly-fluctuating media) it is more practical and it enables to understand the controlling parameters for the stability. It is worth emphasising that this paper focuses on the acoustic case only and considers the SEM with Gauss-Lobatto-Legendre points and the Leap-Frog time integration scheme. However, it is very important to point out that the ideas proposed here are general and they can be directly applied to the analysis of the stability of other SEM methods [25,26] and other time integrators [27,28] within the context of acoustic or elastic wave propagation.

In the next section, the wave equation in a heterogeneous medium is introduced. The discretisation with high-order spectral elements [29,30,31,32] in space and the Leap-Frog scheme in time is described. In Section 3, the stability of the Leap-Frog scheme is considered, and the Irons and Treharne theorem is recalled. This theorem allows to bound the global stability criterion with a maximum over elemental stability criteria. Section 4 presents a stability result for the particular setting of strongly-heterogeneous and/or rapidly-fluctuating media media using an asymptotic analysis. In Section 5, several bounds for the maximum eigenvalue of a general matrix are recalled and compared to obtain computable bounds on the stability in a general heterogeneous medium. The most accurate bounds are identified through extensive numerical experiments in 1D, 2D and 3D in Section 6. Finally, several numerical examples are presented in Section 7 to evaluate the accuracy of the proposed stability criteria both for slowly- and rapidly-fluctuating material properties. In particular, a large scale simulation of wave propagation in a 3D randomly-heterogeneous medium is considered in Section 7.2.

2 | PROBLEM STATEMENT AND DISCRETISATION

2.1 | Weak formulation

Let us consider the acoustic wave equation in a heterogeneous medium $\Omega \subset \mathbb{R}^{\mathtt{n_{sd}}}$ (with $\mathtt{n_{sd}}$ number of spatial dimensions) characterised by a density function $\eta(\boldsymbol{x})$ and a Lamé parameter $\gamma(\boldsymbol{x})$

$$\eta(\boldsymbol{x})\frac{\partial^2 u(\boldsymbol{x},t)}{\partial t^2} - \boldsymbol{\nabla}\cdot(\gamma(\boldsymbol{x})\boldsymbol{\nabla}u(\boldsymbol{x},t)) = f(\boldsymbol{x},t), \quad \text{for } (\boldsymbol{x},t)\in\Omega\times(0,T], \tag{2}$$

where $u(\boldsymbol{x},t)$ is a scalar field and $f(\boldsymbol{x},t)$ denotes a time-dependent source. The problem is closed by considering appropriate initial and boundary conditions, namely

$$u(\boldsymbol{x},0) = u_0(\boldsymbol{x}), \quad \frac{\partial u(\boldsymbol{x},0)}{\partial t} = v_0(\boldsymbol{x}), \qquad \text{for } \boldsymbol{x}\in\Omega. \tag{3}$$

and

$$u(\boldsymbol{x},t) = u_d(t), \quad \text{for } \boldsymbol{x}\in\partial\Omega\times(0,T], \tag{4}$$

where, to simplify the presentation and without loss of generality, only Dirichlet boundary conditions are considered.

The weak statement equivalent to the strong form (2), is obtained by multiplying Equation (2) by a test function $v(\boldsymbol{x})$, integrating in the whole domain and performing an integration by parts of the term with second order spatial derivatives. The resulting weak form reads: find $u(\boldsymbol{x},t)\in\mathcal{W}_t$ such that $u(\boldsymbol{x},t) = u_d(t)$ on $\partial\Omega\times[0,T]$ and

$$\int_\Omega \eta(\boldsymbol{x})v(\boldsymbol{x})\frac{\partial^2 u(\boldsymbol{x},t)}{\partial t^2}d\Omega + \int_\Omega \gamma(\boldsymbol{x})\boldsymbol{\nabla}v(\boldsymbol{x})\cdot\boldsymbol{\nabla}u(\boldsymbol{x},t)d\Omega = \int_\Omega v(\boldsymbol{x})f(\boldsymbol{x},t)d\Omega, \tag{5}$$

for all $v(\boldsymbol{x})\in\mathcal{H}_0^1(\Omega)$, where

$$\mathcal{W}_t = \left\{u \mid u(\cdot,t)\in\mathcal{H}^1(\Omega), t\in[0,T] \text{ and } u(\boldsymbol{x},t)=u_d(\boldsymbol{x},t) \text{ for } (\boldsymbol{x},t)\in\partial\Omega\times[0,T]\right\}. \tag{6}$$

2.2 | Spatial and temporal discretisation

The spatial domain is discretised using $\mathtt{n_{el}}$ disjoint elements Ω_e,

$$\overline{\Omega} = \bigcup_{i=1}^{\mathtt{n_{el}}}\overline{\Omega}_e, \qquad \Omega_e\cap\Omega_l = \emptyset \quad \text{for } e\neq l.$$

In this work, quadrilateral and hexahedral elements are employed in two and three dimensions respectively.

A nodal approximation of the solution is considered in the reference element $\hat{\Omega} = [-1,1]^{\mathtt{n_{sd}}}$, with local coordinates $\boldsymbol{\xi} = (\xi_1,\dots,\xi_{\mathtt{n_{sd}}})$, namely

$$u_h^e(\boldsymbol{\xi},t) = \sum_{j=1}^{\mathtt{n_{en}}} N_j(\boldsymbol{\xi})u_j(t), \tag{7}$$

where N_j are Lagrange polynomials of degree p, u_j denote the time-dependent values of the solution at the nodal points and $\mathtt{n_{en}} = (p+1)^{\mathtt{n_{sd}}}$ is the number of nodes per element. The Lagrange polynomials, defined in the reference element $\hat{\Omega}$, are constructed using the Gauss-Lobatto-Legendre (GLL) points $\boldsymbol{\xi}_j = (\xi_{j,1},\dots,\xi_{j,\mathtt{n_{sd}}})$ and an isoparametric transformation is used to link the reference element $\hat{\Omega}$ and the computational element Ω_e

$$\begin{aligned}\boldsymbol{\varphi}^e \ &: \hat{\Omega}\subset\mathbb{R}^{\mathtt{n_{sd}}} \longrightarrow \Omega_e\subset\mathbb{R}^{\mathtt{n_{sd}}}\\ &\boldsymbol{\xi}\mapsto\boldsymbol{\varphi}^e(\boldsymbol{\xi}) := \sum_{j=1}^{\mathtt{n_{en}}}\boldsymbol{x}_j^e N_j(\boldsymbol{\xi}),\end{aligned} \tag{8}$$

where $\boldsymbol{x}_j^e = \boldsymbol{\varphi}^e(\boldsymbol{\xi}_j)$ are the nodal coordinates of element Ω_e.

Introducing the approximation of the solution in the weak formulation of Equation (5) and selecting the space of the weighting functions to be the same as the space of the interpolation functions, leads to the semi-discrete system of ordinary differential equations

$$\mathbf{M}\frac{d^2\mathbf{U}}{dt^2} + \mathbf{K}\mathbf{U} = \mathbf{F}, \tag{9}$$

where the vector $\mathbf{U}$, of size equal to the total number of mesh nodes ($\mathtt{n_{mn}}$), contains the nodal values of the solution. The mass matrix $\mathbf{M}$, the stiffness matrix $\mathbf{K}$ and the forcing vector $\mathbf{F}$ are computed by assembling the elemental contributions. The elemental

matrices are computed in the reference element after introducing the isoparametric mapping and a numerical quadrature. In the SEM[33,34], the quadrature points are selected to be the same as the nodal points (i.e. the GLL nodal distribution), leading to the following expressions for the elemental mass and stiffness matrices

$$M^e_{ij} = \delta_{ij}\eta^e_i|\mathbf{J}^e_i|\omega_i, \quad K^e_{ij} = \sum_{k=1}^{\mathtt{n}_{\mathtt{en}}} \gamma^e_k \left[(\mathbf{J}^e_k)^{-1}\boldsymbol{\nabla} N_i(\boldsymbol{\xi}_k)\right] \cdot \left[(\mathbf{J}^e_k)^{-1}\boldsymbol{\nabla} N_j(\boldsymbol{\xi}_k)\right] |\mathbf{J}^e_k|\omega_k, \tag{10}$$

where $\eta^e_l = \eta(\boldsymbol{x}^e_l)$ and $\gamma^e_l = \gamma(\boldsymbol{x}^e_l)$ denote the material properties at the node $\boldsymbol{x}^e_l$, ω_l is the GLL quadrature weight of the node $\boldsymbol{\xi}_l$, $\mathbf{J}^e = \partial\boldsymbol{\varphi}^e/\partial\boldsymbol{\xi}$ is the Jacobian of the isoparametric mapping and $\mathbf{J}^e_l = \mathbf{J}^e(\boldsymbol{\xi}_l)$ is the Jacobian evaluated at the GLL point $\boldsymbol{\xi}_l$. It is worth noting that the mass matrix is diagonal because the Lagrange polynomials satisfy the delta Kronecker property, that is $N_i(\boldsymbol{\xi}_j) = \delta_{ij}$. Note also that, in the case of a random medium, the parameters are obtained as realisations of random fields. Considering the parameters only through their value at the nodes may effectively slightly modify the statistics of these random parameters.

Assuming a Cartesian grid with uniform spacing h, the isoparametric transformation reduces to a linear mapping and its Jacobian is simply $\mathbf{J}^e = (h/2)\mathbf{I}_{\mathtt{n}_{\mathtt{sd}}}$. In this case the elemental mass and stiffness matrices reduce to

$$M^e_{ij} = \delta_{ij}\eta^e_i\omega_i \left(\frac{h}{2}\right)^{\mathtt{n}_{\mathtt{sd}}}, \quad K^e_{ij} = \left(\frac{2}{h}\right)^{2-\mathtt{n}_{\mathtt{sd}}} \sum_{k=1}^{\mathtt{n}_{\mathtt{en}}} \left(\gamma^e_k\omega_k \sum_{l=1}^{\mathtt{n}_{\mathtt{sd}}} \frac{\partial N_i(\boldsymbol{\xi}_k)}{\partial\xi_l}\frac{\partial N_j(\boldsymbol{\xi}_k)}{\partial\xi_l} \right). \tag{11}$$

In a one-dimensional problem, the expressions of the elemental matrices for a mesh with uniform spacing h further simplify to

$$M^e_{ij} = \delta_{ij}\eta^e_i\omega_i\frac{h}{2}, \quad K^e_{ij} = \frac{2}{h}\sum_{k=1}^{\mathtt{n}_{\mathtt{en}}} \left(\gamma^e_k\omega_k d_{ki}d_{kj}\right), \tag{12}$$

where $d_{ab} = dN_b(\xi_a)/d\xi$ denote the derivatives of the Lagrange polynomials evaluated at the GLL points, which, according to[35], can be evaluated as

$$d_{ab} = \begin{cases} -\dfrac{1}{4}p(p+1) & \text{if } a = b = 1 \\ \dfrac{P_p(\xi_a)}{(\xi_a - \xi_b)P_p(\xi_b)} & \text{if } a \neq b, 1 \leq a, b \leq p+1 \\ 0 & \text{if } 2 \leq a = b \leq p \\ \dfrac{1}{4}p(p+1) & \text{if } a = b = p+1 \end{cases}, \tag{13}$$

where P_p is the Legendre polynomial of order p.

The main benefit of the SEM is its efficiency when combined with an explicit time marching algorithm. In this work, the classical second-order accurate Leap-Frog scheme is considered. At each time step the solution is advanced in time according to

$$\mathbf{U}^{n+1} = 2\mathbf{U}^n - \mathbf{U}^{n-1} + \Delta t^2\mathbf{M}^{-1}\left(\mathbf{F}^n - \mathbf{K}\mathbf{U}^n\right), \tag{14}$$

where it is worth emphasizing that in the context of the SEM, each time step only involves the solution of a trivial system of equations with diagonal mass matrix.

3 | STABILITY OF THE LEAP-FROG SCHEME

The stability analysis of the discrete scheme given by Equation (14) shows that the SEM with the Leap-Frog time discretisation is only conditionally stable[5]. The so-called Courant-Friedrichs-Levy (CFL) stability condition can be written as

$$\Delta t \leq \frac{2}{\sqrt{\lambda_{\max}}}, \tag{15}$$

where $\lambda_{\max}$ is the maximum eigenvalue of the dispersion matrix $\mathbf{D} := \mathbf{M}^{-1}\mathbf{K}$.

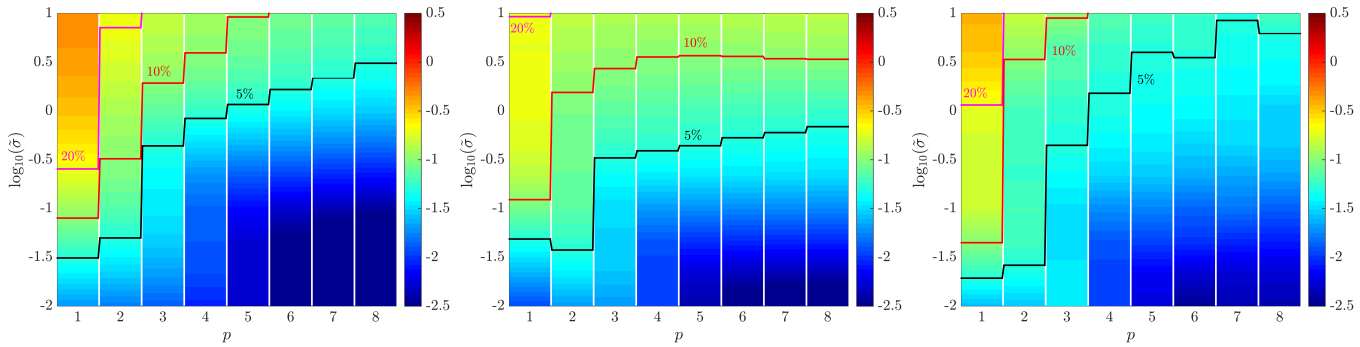

(a) 1D (b) 2D (c) 3D

FIGURE 1 Relative difference between the maximum of $\lambda^e_{\max}$ for all the elemental dispersion matrices and the maximum eigenvalue of the global dispersion matrix in logarithmic scale for different values of the degree of approximation and the variance of the material properties.

3.1 | The theorem of Irons and Treharne

As described in [36,24,37] for the finite element and spectral element methods (and other methods for which the matrices are obtained by assembling elemental contributions), the eigenvalues λ_m, for $m = 1, \dots, \mathtt{n}_{\mathtt{mn}}$, of $\mathbf{D}$ are bounded by

$$\min_{\Omega_e} \lambda^e_{\min} \leq \lambda_m \leq \max_{\Omega_e} \lambda^e_{\max}, \qquad \text{for } m = 1, \dots, \mathtt{n}_{\mathtt{mn}}, \tag{16}$$

where $\lambda^e_{\min}$ and $\lambda^e_{\max}$ are the minimum and maximum eigenvalues of the elemental matrix $\mathbf{D}^e := (\mathbf{M}^e)^{-1}\mathbf{K}^e$ respectively. This is known as the theorem of Irons and Treharne and it implies that

$$\lambda_{\max} \leq \max_{\Omega_e} \lambda^e_{\max}. \tag{17}$$

Therefore, a conservative choice for the time step that ensures stability is

$$\Delta t \leq \frac{2}{\sqrt{\max_{\Omega_e} \lambda^e_{\max}}} \leq \frac{2}{\sqrt{\lambda_{\max}}}. \tag{18}$$

3.2 | Sharpness of the Irons and Treharne bound for heterogeneous media

The theorem of Irons and Treharne has been previously applied to compute a time step that ensures stability of an explicit time integrator scheme in applications with homogeneous materials and by using different numerical techniques, e.g. the standard finite element method [38], the boundary element method [39] and the natural element method [40]. The same idea has also been exploited to study the effect of element distortion in the stability of a finite element method using two-dimensional quadrilateral elements [37]. To the knowledge of the authors, the application of the Irons and Treharne theorem has not been previously considered for heterogeneous media.

To illustrate the sharpness of the bound of the maximum eigenvalue provided by the Irons and Treharne theorem, Figure 1 shows the error, in logarithmic scale, between the maximum of $\lambda^e_{\max}$ for all the elemental dispersion matrices and the maximum eigenvalue of the global dispersion matrix, $\lambda_{\max}$, defined as

$$\epsilon_{\mathtt{IT}} = \frac{\max_{\Omega_e} \lambda^e_{\max} - \lambda_{\max}}{\lambda_{\max}}. \tag{19}$$

The mechanical parameters γ and η at the nodes are modelled as realisations of log-normal random variables with average $\mu = 2$ and variance $\sigma^2 = (\tilde{\sigma}\mu)^2$, where $\tilde{\sigma} \in [0.01, 10]$. The results in Figure 1 display the mean value of $\epsilon_{\mathtt{IT}}$ for a degree of approximation p ranging from 1 to 8.

In one dimension, a mesh with 40 equally-spaced elements is used. In two and three dimensions, a Cartesian grid with 100 and 512 equally-sized elements, respectively, is considered. In all cases the number of realisations of the mechanical properties is increased until the results do not present a sizeable difference by adding more realisations.

It is worth noting that the value of ϵ_{IT} is always positive, as expected due to the theorem of Irons and Treharne (17). In one dimension, only for linear elements (i.e. $p = 1$) and large values of $\tilde{\sigma}$, an error above 20% is observed, whereas for the large majority of degrees of approximations and values of $\tilde{\sigma}$ considered, a value of ϵ_{IT} below 5% is obtained. It is also important to observe how the range of values of $\tilde{\sigma}$ where an accurate result is obtained, increases as the degree of approximation is increased.

In two and three dimensions accurate results, with a value of ϵ_{IT} below 20%, are observed for all degrees of approximation and all values of $\tilde{\sigma}$ considered except for linear elements and a high value of the variance. In two dimensions a value of ϵ_{IT} below 10% is obtained for a low to moderate value of $\tilde{\sigma}$, whereas in three dimensions the accuracy is higher, with a value of ϵ_{IT} below 10% for almost all values of the variance of the material properties considered.

4 | STIFF-VERTEX STABILITY CRITERION FOR STRONGLY-HETEROGENEOUS AND/OR RAPIDLY-FLUCTUATING MEDIA

This Section presents a stability criterion for heterogeneous media derived using asymptotic analysis for the particular case of strongly-heterogeneous and/or rapidly-fluctuating material properties. More precisely, the criterion derived in this Section assumes that the local velocity at one element node is much higher than the local velocity in the rest of the nodes. This situation is typical encountered in random media with a correlation length relatively small compared to the element size (or even white noise) and in random media with a relatively large variance.

Let us consider a small parameter ϵ and assume that in the i-th GLL node of one element the stiffness is large ($\gamma_i^e = \mathcal{O}(\epsilon^{-1})$) and the density is small ($\eta_i^e = \mathcal{O}(\epsilon)$), where the material parameters in all other nodes of the element are $\mathcal{O}(1)$. Using the definition of the elemental mass and stiffness matrices in Equation (11), it is clear that this assumption implies that the elements $\mathbf{K}_{ij}^e = \mathcal{O}(\epsilon^{-1})$, for any $1 \leq j \leq \mathtt{n}_{\mathtt{en}}$, whereas the diagonal element $\mathbf{M}_{ii}^e = \mathcal{O}(\epsilon)$. Under this assumption, the largest eigenvalue of the dispersion matrix can be written as

$$\lambda_{\max}^e = \left(\frac{2c_i^e}{h}\right)^2 \sum_{l=1}^{\mathtt{n}_{\mathtt{sd}}} \left(\frac{\partial N_i(\boldsymbol{\xi}_i)}{\partial \xi_l}\right)^2 + \mathcal{O}(\epsilon^{-1}) = \left(\frac{2c_i^e}{h}\right)^2 n_{\text{geom}}^{\mathtt{n}_{\mathtt{sd}}} \left(\frac{p(p+1)}{4}\right)^2 + \mathcal{O}(\epsilon^{-1}). \tag{20}$$

where $c_i^e = \sqrt{\gamma_i^e/\eta_i^e} = \mathcal{O}(\epsilon^{-1})$ is the velocity at the i-th GLL node and the second equality in Equation (20) is obtained by using Equation (13) and the tensorised definition of the Lagrange polynomials in multiple dimensions. In three dimensions, $n_{\text{geom}}^3 = 3$ if the i-th node is an element vertex, $n_{\text{geom}}^3 = 2$ if the i-th node is located on an element edge, $n_{\text{geom}}^3 = 1$ if the i-th node is located on an element face and $n_{\text{geom}}^3 = 0$ if the i-th node is interior to the element. Similarly, in two dimensions, $n_{\text{geom}}^2 = 2$ if the i-th node is an element vertex, $n_{\text{geom}}^2 = 1$ if the i-th node is located on an element edge and $n_{\text{geom}}^2 = 0$ otherwise.

Equation (20) implies that $\lambda_{\max}^e = \mathcal{O}(\epsilon^{-2})$ if $\boldsymbol{x}_i \notin \partial\Omega_e$, that is when the extreme value of the velocity is found in a node interior to the element, whereas $\lambda_{\max}^e = \mathcal{O}(\epsilon^{-1})$ if $\boldsymbol{x}_i \in \partial\Omega_e$. Furthermore, the maximum eigenvalue is largest when the extreme value of the velocity is found on the vertices of the element.

For large scale simulations that require a mesh with a large number of elements, it is reasonable to assume that the maximum eigenvalue will be controlled by the elemental maximum eigenvalue in an element where the extreme velocity is found on a vertex of the element. Using the Irons and Treharne theorem, and observing that for vertices $n_{\text{geom}}^{\mathtt{n}_{\mathtt{sd}}} = \mathtt{n}_{\mathtt{sd}}$, the following estimate of the maximum eigenvalue of the global dispersion matrix is obtained

$$\lambda_{\max} \approx \lambda^{\mathtt{SV},0} = \mathtt{n}_{\mathtt{sd}} \left(\frac{c_{\max}^V}{h} \frac{p(p+1)}{2}\right)^2, \tag{21}$$

where $c_{\max}^V$ is the maximum velocity over all the vertices of the mesh (i.e. not all the mesh nodes) and $\mathtt{SV}$ refers to "Stiff Vertex". The global stability criterion can be taken as

$$\Delta t^{\mathtt{SV},0} \leq \frac{h}{c_{\max}^V} \frac{4}{p(p+1)\sqrt{\mathtt{n}_{\mathtt{sd}}}}, \tag{22}$$

Remark 1. The bound of Equation (22) features the coefficient $1/\sqrt{\mathtt{n}_{\mathtt{sd}}}$ that appears in the classical stability limit derived for homogeneous media[5]. The result is also consistent with the stability limit found in[18] under a very different setting (i.e. stability limit for quadratic spectral elements in a medium with periodically-fluctuating material properties).

The values of the stability criterion $\alpha_M^{\mathtt{SV},0} := 4/(p(p+1)\sqrt{\mathtt{n}_{\mathtt{sd}}}$ are presented in Table 2 and compared to those of the stability criterion α_M for a homogeneous medium in Table 1 in one dimension. Despite the value obtained in this Section seems to lead

to a larger allowable time step, it is important to note that this is because the criterion derived here is *a priori* associated to a larger velocity ($c^V_{\max}$ is assumed to be much larger than the velocity at nodes that are not vertices).

TABLE 2 One-dimensional stiff-vertex stability criterion $\alpha_M^{\mathtt{SV},0}$ for spectral elements of polynomial order p and ratio between $\alpha_M^{\mathtt{SV},0}$ and the classical stability criterion α_M (see Table 1) for a homogeneous medium.

	p=1	p=2	p=3	p=4	p=5
$\alpha_M^{\mathtt{SV},0}$	2.00	0.66	0.33	0.20	0.13
$\alpha_M^{\mathtt{SV},0}/\alpha_M$	2.00	1.67	1.45	1.43	1.33

Remark 2. It is worth emphasising that the stability criterion of Equation (22) is not conservative and, therefore, cannot be used in practice. This has been confirmed with numerical examples not reported here for brevity. However, its simple definition offers an insight into the possible causes for obtaining a too conservative time step when the criterion derived for homogeneous media is adapted for the heterogeneous case. First, α_M leads to a more conservative time step when compared to $\alpha_M^{\mathtt{SV},0}$. Second, the modification of the stability limit derived for homogeneous media uses the maximum velocity over all the mesh nodes and not over the mesh vertices as done when the stability limit of Equation (22) is considered.

Remark 2 indicates that, to obtain a conservative estimate of the stability limit, it is necessary to go beyond the leading-order asymptotic analysis. This is done in the following proposition.

Proposition 1 (Elemental eigenvalue in a rapidly-fluctuating random medium)**.** Let us consider a small parameter ϵ and assume that in the i-th GLL node of one element the stiffness is large ($\gamma_i^e = \mathcal{O}(\epsilon^{-1})$) and the density is small ($\eta_i^e = \mathcal{O}(\epsilon)$), where the material parameters in all other nodes of the element are $\mathcal{O}(1)$. The maximum eigenvalue of the elemental dispersion matrix $\mathbf{D}^e = (\mathbf{M}^e)^{-1}\mathbf{K}^e$ is, asymptotically,

$$\lambda^e_{\max} = \mathrm{tr}(\mathbf{D}^e) + \mathcal{O}(\epsilon^{-1}) \tag{23}$$

In addition, the following upper bound of the maximum eigenvalue of the elemental dispersion matrix holds true

$$\lambda^e_{\max} \leq \mathrm{tr}(\mathbf{D}^e) \tag{24}$$

Proof. See Appendix A. □

Using the Irons and Treharne theorem, the bound of the maximum elemental eigenvalue of the elemental dispersion matrix of Equation (24) leads to the the following conservative stability criterion

$$\Delta t \leq \Delta t^{\mathtt{SV},1} = \frac{2}{\sqrt{\mathrm{tr}(\mathbf{D}^e)}}. \tag{25}$$

As it will be shown in the numerical examples in Section 7, the stability criterion of Equation (25) is conservative but it will not always provide an accurate estimate of the stability limit, especially when the material properties fluctuate slowly or when the variance of the fluctuation decreases. More general eigenvalue bounds are described in the next section.

5 | STABILITY CRITERIA BASED ON EIGENVALUE BOUNDS

As explained in Section 3, the theorem of Irons and Treharne can be used to obtain a conservative estimate of the critical time step with randomly fluctuating heterogeneous media. However, the use of Equation (18) to define a stable time step requires the computation of the maximum eigenvalue of all the elemental dispersion matrices. For linear elements, an analytical computation of the eigenvalues of the elemental matrices is feasible in one and two dimensions, but for high-order spectral elements in three dimensions, the computation of the exact eigenvalue of the elemental matrices is not considered a practical option. In this Section, a number of eigenvalue bounds are considered as a viable alternative to estimate the maximum eigenvalue of the elemental dispersion matrices. The cost of evaluating these bounds is also discussed in Section 5.2.2.

5.1 | Eigenvalue bounds

There is an extensive list of results involving bounds of eigenvalues or linear combinations of eigenvalues of random complex matrices[41,42]. In this Section, some of the results available in the literature are recalled for the particular case of the bound of the maximum eigenvalue of a real matrix. A simple optimality criterion for these bounds is discussed in Appendix B. This criterion indicates whether the bound is optimal for linear spectral elements in one-dimension.

5.1.1 | Frobenius' bound

A classical result of a bound of the eigenvalues of a matrix in terms of its elements is given by Frobenius' theorem[41]. A consequence of this theorem is the following upper bound of the maximum eigenvalue of a square matrix $\mathbf{A} \in \mathbb{R}^{n\times n}$

$$\lambda_{\mathtt{F}}(\mathbf{A}) = \min\left\{ \max_{i=1,\dots,n}\left\{ \sum_{j=1}^{n} |A_{ij}| \right\}, \max_{j=1,\dots,n}\left\{ \sum_{i=1}^{n} |A_{ij}| \right\} \right\}. \tag{26}$$

Remark 3. One of the most popular results related to the bounds of matrix eigenvalues is due to Lévy, Hadamard and Gerschgorin[42,43]. A consequence of the so-called Lévy-Hadamard-Gerschgorin theorem is that an upper bound of the maximum eigenvalue of a square matrix $\mathbf{A} \in \mathbb{R}^{n\times n}$ is given by

$$\lambda_{\mathtt{LHG}}(\mathbf{A}) = \max_{i=1,\dots,n}\left\{ A_{ii} + P_i(\mathbf{A}) \right\}, \tag{27}$$

where

$$P_k(\mathbf{A}) = \sum_{\substack{l=1 \\ l\neq k}}^{n} |A_{kl}|. \tag{28}$$

In general it is not possible to establish if the Frobenius' bound is sharper than the Lévy-Hadamard-Gerschgorin bound. However, when applied to an elemental dispersion matrix, it can be easily shown that the Frobenius' bound is sharper than the bound derived from the Lévy-Hadamard-Gerschgorin theorem. As the diagonal terms of the dispersion matrix are non-negative, the Lévy-Hadamard-Gerschgorin bound can be written as

$$\lambda_{\mathtt{LHG}}(\mathbf{D}^e) = \max_{i=1,\dots,n}\left\{ \sum_{j=1}^{n} |D^e_{ij}| \right\}. \tag{29}$$

From Equations (29) and (26) it can be easily observed that

$$\lambda_{\mathtt{F}}(\mathbf{D}^e) = \min\left\{ \lambda_{\mathtt{LHG}}(\mathbf{D}^e), \lambda_{\mathtt{LHG}}\left((\mathbf{D}^e)^T\right) \right\} \leq \lambda_{\mathtt{LHG}}(\mathbf{D}^e). \tag{30}$$

5.1.2 | Parkers' bound

Another bound, considered a refinement of an early result by Browne[42], provides the following upper bound of the maximum eigenvalue of a square matrix $\mathbf{A} \in \mathbb{R}^{n\times n}$

$$\lambda_{\mathtt{P}}(\mathbf{A}) = \frac{1}{2}\max_{i=1,\dots,n}\left\{ \sum_{j=1}^{n} \left(|A_{ij}| + |A_{ji}| \right) \right\}. \tag{31}$$

5.1.3 | Ostrowski's bound

The next result, similar to the Frobeniu's bound, is a consequence of the work by Ostrowski[41] and provides the following upper bound of the maximum eigenvalue of a square matrix $\mathbf{A} \in \mathbb{R}^{n\times n}$

$$\lambda_{\mathtt{O}}(\mathbf{A}) = \min_{\beta\in[0,1]}\left\{ \max_{i=1,\dots,n}\left\{ A_{ii} + \left(P_i(\mathbf{A})\right)^{\beta}\left(P_i(\mathbf{A}^T)\right)^{1-\beta} \right\} \right\}. \tag{32}$$

5.1.4 | Brauer's bound

The work by Brauer[44] extending the results by Lévy, Hadamard and Gerschgorin led to another well known bound for the eigenvalues. For a square matrix $\mathbf{A} \in \mathbb{R}^{n\times n}$, the following upper bound is a consequence of Brauer's work:

$$\lambda_{\mathtt{B}}(\mathbf{A}) = \frac{1}{2} \max_{\substack{i,j=1,\dots,n \\ i\neq j}} \left\{ |A_{ii}| + |A_{jj}| + \sqrt{\left(|A_{ii}| - |A_{jj}|\right)^2 + 4P_i(\mathbf{A})P_j(\mathbf{A})} \right\}. \tag{33}$$

5.1.5 | Trace bound

Another family of well known results for the bounds of eigenvalues involves the use of the trace of the matrix and the trace of its square[45]. For a square matrix $\mathbf{A} \in \mathbb{R}^{n\times n}$, the following upper bound is a consequence of[46]

$$\lambda_{\mathtt{T}}(\mathbf{A}) = \bar{\lambda}(\mathbf{A}) + \sigma(\mathbf{A})\sqrt{n-1}, \tag{34}$$

where $\bar{\lambda}(\mathbf{A})$ and $\sigma(\mathbf{A})$ are the mean and standard deviation of the eigenvalues of $\mathbf{A}$ respectively[45], which can be expressed in terms of the trace of $\mathbf{A}$ and the trace of $\mathbf{A}^2$ as

$$\bar{\lambda}(\mathbf{A}) = \frac{1}{n}\mathrm{tr}(\mathbf{A}), \qquad \sigma(\mathbf{A}) = \sqrt{\frac{1}{n}\mathrm{tr}(\mathbf{A}^2) - \bar{\lambda}^2}. \tag{35}$$

5.2 | Computability of the eigenvalue bounds for SEM elemental matrices

This section briefly discusses the computability of closed-form expressions for the stability criteria derived from the theorem of Irons and Treharne combined with the eigenvalue bounds presented in Section 5.1. The computational cost of evaluating these expressions is also discussed and compared to the computational cost required by the classical power method commonly used to approximate the maximum eigenvalue of a diagonalisable matrix.

5.2.1 | Closed-form expressions for the eigenvalue bounds

Out of the five eigenvalue bounds considered in this work, four of them require the computation of the absolute value of the dispersion matrix terms, that can be written as

$$|D^e_{ij}| = \frac{|K^e_{ij}|}{M^e_{ii}} = \frac{4}{h^2\eta^e_i\omega_i} \left| \sum_{k=1}^{\mathtt{n_{en}}} \left(\gamma^e_k\omega_k \sum_{l=1}^{\mathtt{n_{sd}}} \frac{\partial N_i(\boldsymbol{\xi}_k)}{\partial \xi_l} \frac{\partial N_j(\boldsymbol{\xi}_k)}{\partial \xi_l} \right) \right|. \tag{36}$$

This absolute value can be easily computed for the elemental dispersion matrices to evaluate the first four eigenvalue bounds described in Section 5.1.

The computation of the trace bound requires the evaluation of the trace of the dispersion matrix and its square, which can be expressed as

$$\mathrm{tr}(\mathbf{D}^e) = \frac{4}{h^2} \sum_{i=1}^{\mathtt{n_{en}}} \left\{ \frac{1}{\eta^e_i\omega_i} \sum_{k=1}^{\mathtt{n_{en}}} \left[\gamma^e_k\omega_k \sum_{l=1}^{\mathtt{n_{sd}}} \left(\frac{\partial N_i(\boldsymbol{\xi}_k)}{\partial \xi_l} \right)^2 \right] \right\}. \tag{37}$$

$$\mathrm{tr}\left((\mathbf{D}^e)^2\right) = \frac{16}{h^4} \sum_{i=1}^{\mathtt{n_{en}}} \left\{ \frac{1}{\eta^e_i\omega_i} \sum_{j=1}^{\mathtt{n_{en}}} \frac{1}{\eta^e_j\omega_j} \left[\sum_{k=1}^{\mathtt{n_{en}}} \left(\gamma^e_k\omega_k \sum_{l=1}^{\mathtt{n_{sd}}} \frac{\partial N_i(\boldsymbol{\xi}_k)}{\partial \xi_l} \frac{\partial N_j(\boldsymbol{\xi}_k)}{\partial \xi_l} \right) \right]^2 \right\}. \tag{38}$$

Again, these quantities can be easily computed for the elemental dispersion matrices to evaluate the trace bound within an existing SEM solver.

5.2.2 | Computational cost

The computation of each eigenvalue bound recalled in the previous Section requires $\mathcal{O}(\mathtt{n}^2_{\mathtt{en}})$ floating point operations (FLOPS). It is worth noting that the classical power method to approximate the maximum eigenvalue of a matrix has also $\mathcal{O}(\mathtt{n}^2_{\mathtt{en}})$ FLOPS. Therefore, it is of interest to compare the FLOPS required by both approaches. To this end, all the FLOPS are considered here, including lower order terms that are not usually considered when an asymptotic analysis is performed. This is considered crucial to compare the performance as the size of the elemental dispersion matrices is relatively small compared to the size of a global matrix.

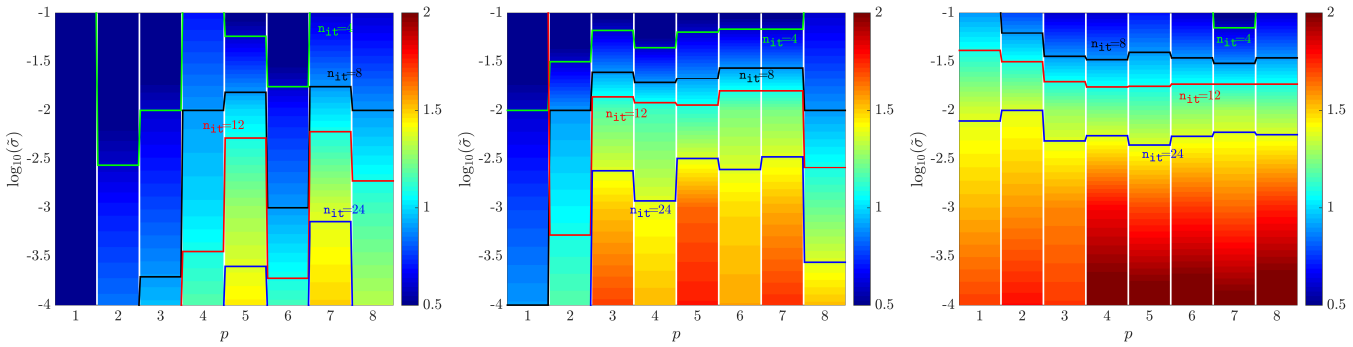

(a) 1D (b) 2D (c) 3D

FIGURE 2 mean value of the number of iterations, in logarithmic scale, required by the power method to compute the eigenvalue of the dispersion matrix with a tolerance of $\epsilon_{\texttt{PM}}$.

The count of the FLOPS required by the expressions is given by

$$\begin{aligned}
\text{FLOPS}_{\texttt{F}} &= 3\texttt{n}_{\texttt{en}}^2 - \texttt{n}_{\texttt{en}} + 1 \\
\text{FLOPS}_{\texttt{P}} &= 3\texttt{n}_{\texttt{en}}^2 + 1 \\
\text{FLOPS}_{\texttt{0}} &= 3\texttt{n}_{\texttt{en}}^2 - 2\texttt{n}_{\texttt{en}} \quad , \\
\text{FLOPS}_{\texttt{B}} &= 4\texttt{n}_{\texttt{en}}^2 - 7\texttt{n}_{\texttt{en}} + 9 \\
\text{FLOPS}_{\texttt{T}} &= 2\texttt{n}_{\texttt{en}}^2 + \texttt{n}_{\texttt{en}} + 3
\end{aligned} \tag{39}$$

where $\text{FLOPS}_{\square}$ denotes the FLOPS required to evaluate $\lambda_{\square}(\mathbf{D}^e)$. These results clearly indicate that the trace bound is the one requiring less FLOPS, whereas the Brauer's bound is the one inducing more FLOPS. As many operations required to compute the bounds are shared (i.e. evaluating the absolute values and summing over rows and columns), the FLOPS required to evaluate all the bounds are actually lower than the sum of the FLOPS obtained by evaluating each bound separately. More precisely, the FLOPS required to evaluate all the bounds is $\text{FLOPS}_{\texttt{Bounds}} = 6\texttt{n}_{\texttt{en}}^2 + 3\texttt{n}_{\texttt{en}} + 16$.

For the classical power method, the FLOPS are given by $\text{FLOPS}_{\texttt{PM}} = (2\texttt{n}_{\texttt{en}}^2 + 5\texttt{n}_{\texttt{en}})\texttt{n}_{\texttt{it}}$, where $\texttt{n}_{\texttt{it}}$ is the number of iterations required to obtain an approximation of the maximum eigenvalue with a desired accuracy. It is worth noting that a single iteration of the power method is already more computationally expensive than the evaluation of the trace bound, two iterations are more expensive than the evaluation of any of the other bounds. When the power method requires three or more iterations, the computational cost of evaluating all the eigenvalue bounds is lower than the cost of the power method.

To obtain a quantitative measure of the FLOPS of the power method, Figure 2 shows the mean value of the number of iterations, in logarithmic scale, required to compute the maximum eigenvalue of the dispersion matrix for different orders of polynomials and for different values of the desired error in the eigenvalue. Three lines highlighted in the colour plot represent the accuracy provided by the power method with $\texttt{n}_{\texttt{it}} = 4$, $\texttt{n}_{\texttt{it}} = 8$ and $\texttt{n}_{\texttt{it}} = 12$ iterations. The results reveal that with four iterations and for certain values of the degree of approximation, the accuracy of the power methods is above 10%. In practice this error could lead to an overestimate of the maximum eigenvalue and, consequently, to unstable simulations, if used to define the time step in a simulation. In addition, this computation is already more expensive than evaluating all the eigenvalue bounds.

For one-dimensional problems, increasing the number of iterations of the power method to $\texttt{n}_{\texttt{it}} = 8$ leads to a substantial increase in the accuracy of the computed eigenvalue, but for higher dimensional problems the gain in accuracy is less substantial. For instance, in three-dimensional problems an error of 10% in the maximum eigenvalue is still obtained for some degrees of approximation and, even with $\texttt{n}_{\texttt{it}} = 12$ the error is still close to 9% for some degrees of approximation. This indicates that, for three-dimensional problems, the use of the power method is more expensive than computing all the bounds described in Section 5. Further numerical experiments reveal that, to guarantee a 1% error of the eigenvalues computed with the power method in three dimensions, at least 24 iterations are required. This makes the computation of the eigenvalue with the power method 24 times more expensive than evaluating the trace bound, 16 times more expensive than evaluating the Frobenius' or the Ostrowski's bounds and 8 times more expensive than evaluating all the bounds.

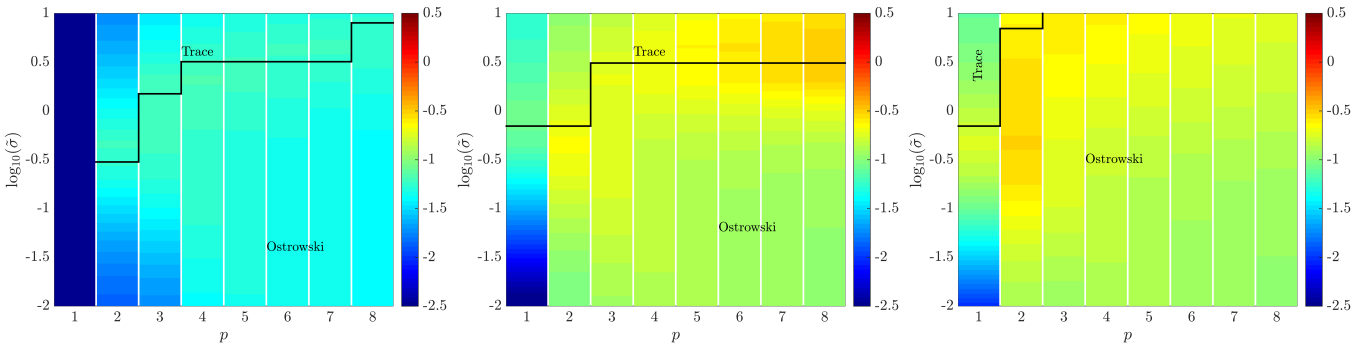

(a) 1D (b) 2D (c) 3D

FIGURE 3 Mean value of the relative difference between the maximum eigenvalue of the elemental dispersion matrix and the best eigenvalue bound in logarithmic scale. The mechanical parameters are modelled as 10,000 realisations of log-normal random variables with average $\mu = 2$, variance $\sigma^2 = (\tilde{\sigma}\mu)^2$ and correlation length $\ell = 2h$.

Remark 4. It is worth emphasising that, strictly speaking, the use of the power method does not guarantee an estimate of the maximum eigenvalue that leads to a stable time step. This is due to the inability to determine if the estimated eigenvalue is less than or greater than the exact eigenvalue.

6 | BEST EIGENVALUE BOUNDS

As shown in Appendix B, some of the eigenvalue bounds presented in Section 5.1 are not optimal, even for linear elements, in a one-dimensional heterogeneous medium. In addition, the bounds that are optimal in this particular case, are not optimal for higher order elements. From the point of view of the stability of the Leap-Frog scheme, it is of interest to know the error induced by the eigenvalue bounds when estimating the maximum eigenvalue of the dispersion matrix of high-order spectral elements.

The mechanical parameters γ and η at the nodes are modelled as realisations of log-normal random variables with average $\mu = 2$, variance $\sigma^2 = (\tilde{\sigma}\mu)^2$, where $\tilde{\sigma} \in [0.01, 10]$ and correlation length $\ell = 2h$, where h is the characteristic element size. A total of 10,000 realisations of the material parameters are considered and, for each realisation, the relative difference between the maximum eigenvalue of the elemental dispersion matrix and the bounds presented in Section 5.1, defined as

$$\epsilon_{\texttt{Bound}} = \log_{10}\left(\frac{\lambda_{\texttt{Bound}}(\mathbf{D}^e) - \lambda^e_{\max}}{\lambda^e_{\max}}\right), \tag{40}$$

is measured.

Figure 3 shows the the mean value of the relative difference, in logarithmic scale, between the maximum eigenvalue of an elemental dispersion matrix and the best of the eigenvalue bounds presented in Section 5.1. In the plots, the regions where one eigenvalue bound provides the best estimate of the exact maximum eigenvalue are highlighted.

The results show a maximum difference of 14%, 16% and 20% for one, two and three-dimensional problems respectively, showing that the accuracy of the bounds is only slightly dependent upon the dimensionality of the problem. In addition, the numerical experiments reveal that the Ostrowski's bound seems to be the most competitive overall. In one dimension, the trace bound provides the most accurate results for a high value of the variance whereas the Ostrowski's bound is more accurate for lower value of the variance. In two and three dimensions, the Ostrowski's bound provides the most accurate results for all values of the variance and all degrees of approximation. It is worth noting that , in both cases, the Ostrowski's and Frobenius' bounds provide identical results for certain values of the variance and the degree of the approximation.

To illustrate the effect of the correlation length ℓ in this study, Figure 4 shows the same study when the correlation length is $\ell = h/5$. The results reveal that the regions and the best eigenvalue bounds are similar for values of the correlation length $\ell = 2h$ and $\ell = h/5$. Note that, in three dimensions and for large values of the variance, the eigenvalue bounds provide more accurate results for a shorter correlation length.

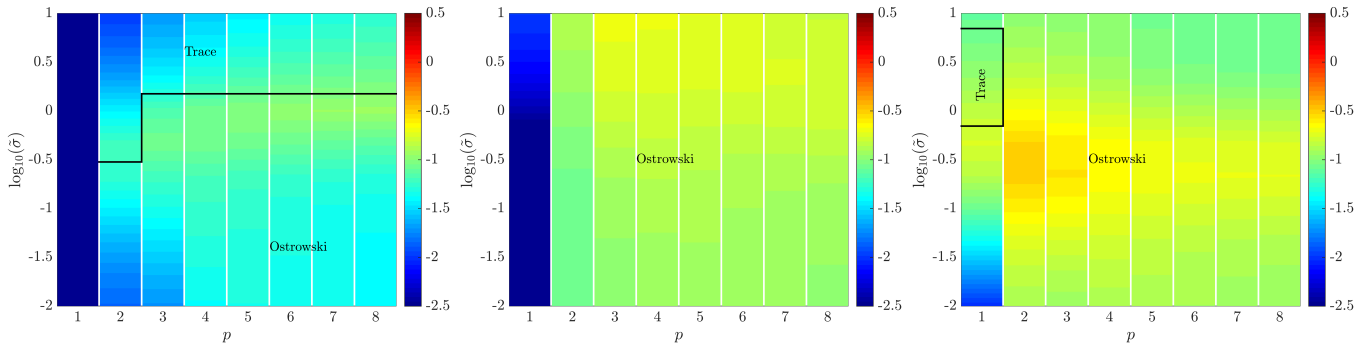

(a) 1D (b) 2D (c) 3D

FIGURE 4 Mean value of the relative difference between the maximum eigenvalue of the elemental dispersion matrix and the best eigenvalue bound in logarithmic scale The mechanical parameters are modelled as 10,000 realisations of log-normal random variables with average $\mu = 2$, variance $\sigma^2 = (\tilde{\sigma}\mu)^2$ and correlation length $\ell = h/5$.

It is worth noting that the results provide a qualitative behaviour of the eigenvalue bounds presented in Section 5.1 but they cannot be used to discard any of the bounds because only the mean value is considered. For completeness, Appendix C shows the results for each one of the eigenvalue bounds that were used to produce the plots in Figure 3 .

7 | NUMERICAL EXAMPLES

This Section presents a number of examples in one and three dimensions to illustrate the accuracy of the stability limit computed from the Irons and Treharne bound and the eigenvalue bounds presented in Section 5.1 as well as the stiff-vertex stability criterion for strongly-heterogeneous and/or rapidly-fluctuating media derived in Section 4.

7.1 | One-dimensional examples

The numerical solution of the model problem given by Equation (2) is considered in $\Omega = [0, 1]$. The material parameters γ and η correspond to realisations of log-normal random variables with average μ, variance $\sigma^2 = (\tilde{\sigma}\mu)^2$ and correlation length ℓ.

The first set of examples considers a mesh with 40 elements and $p = 3$. Five realisations of the material parameters, depicted in Figure 5 (a), are considered with $\mu = 2$, $\tilde{\sigma} = 1$ and $\ell = 2h$, where h denotes the characteristic element size. The blue circles

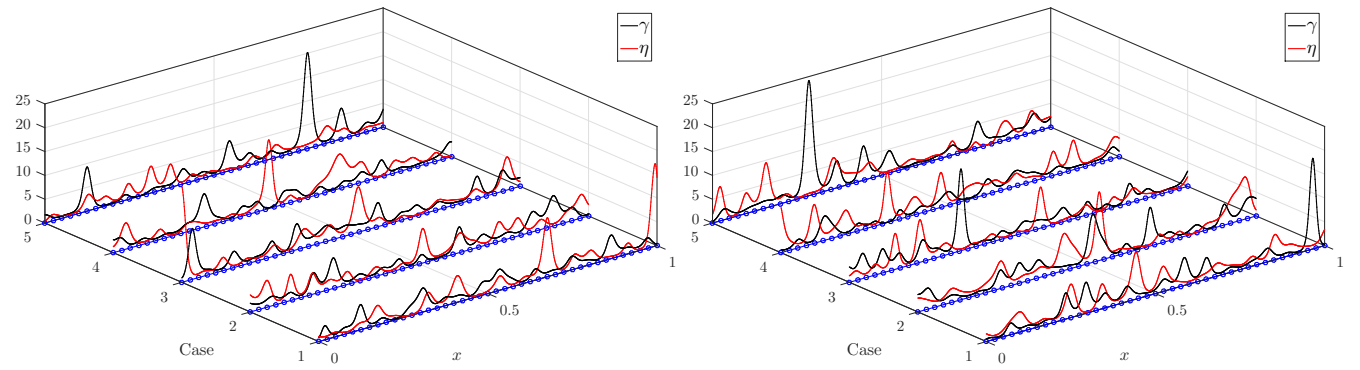

(a) $p = 3$ (b) $p = 5$

FIGURE 5 Realizations of the material parameters with $\mu = 2$, $\tilde{\sigma} = 1$ and $\ell = 2h$.

in Figure 5 (a) denote the nodes of the computational mesh.

For the five realisations in Figure 5 (a), Table 3 reports the exact stability limit, computed as $\Delta t_{\text{Ex}} = 2/\sqrt{\lambda_{\max}}$, the estimate of the stability limit computed by assuming a homogeneous material[47,48], $\Delta t_{\text{H}} = \alpha_M h / \max_i\{c_i\}$, with α_M taken from Table 1 , the stability limit derived from the Irons and Treharne bound, $\Delta t_{\text{IT}} = 2/\sqrt{\max_{\Omega_e} \lambda^e_{\max}}$ and the stability limits obtained by combining the Irons and Treharne bound and eigenvalue bounds of Section 5.1. In Table 3 , the black bold font highlights the

Case	Δt_{Ex}	Δt_{H}	Δt_{IT}	Δt_{F}	Δt_{P}	Δt_{O}	Δt_{B}	Δt_{T}
1	**0.001025**	0.000913	**0.001025**	0.000980	0.000863	0.001018	0.000993	**0.001023**
2	**0.002237**	**0.001769**	**0.002187**	0.001905	0.002040	**0.002154**	0.001854	0.001984
3	**0.001469**	0.001234	**0.001469**	0.001381	0.001210	0.001454	0.001412	**0.001469**
4	**0.001119**	**0.000674**	**0.001035**	0.000900	0.000934	**0.000976**	0.000892	0.000930
5	**0.001587**	**0.001709**	**0.001533**	0.001289	0.001317	**0.001480**	0.001264	0.001454

TABLE 3 Exact stability limit (Δt_{Ex}) compared to the estimate using the homogeneous material bound (Δt_{H}), the bound obtained by the theorem of Irons and Treharne (Δt_{IT}) and the bounds induced by the combination of the theorem of Irons and Treharne and the eigenvalue bounds presented in Section 5.1 for the realisations of the material parameters shown in Figure 5 (a).

exact stability limit, the blue font indicates the Irons and Treharne bound, which is the best possible result to be obtained when the Irons and Treharne is combined with the eigenvalue bounds of Section 5.1. In green, the best estimate of the stability limit using the strategy proposed in this paper is highlighted. In red, the cases where the stability limit computed by assuming a homogeneous material results in an instability is highlighted. Finally, the cases where the stability limit computed by assuming a homogeneous material results in a very conservative estimate (i.e. times step 20% lower than the exact stability limit) are highlighted in orange.

The first case in Table 3 shows a situation where the Irons and Treharne bound produces an almost exact estimate of the maximum eigenvalue. The best estimate using eigenvalue bounds is provided by the trace bound, resulting in a time step only 0.2% lower than the exact stability limit. The Ostrowski's bound also provides an accurate estimate of the stability limit, 0.7% lower than the exact value. The Frobenius' and Brauers' bounds also lead to good estimates, 4% and 3% lower than the exact value, respectively. For this example, the results obtained by considering the estimate derived for homogeneous media results in an approximation of the time step 11% lower than the exact stability limit.

For the second case, the use of the Ostrowski's bound produces the best estimate of the stability limit, with a time step 4% lower than the exact value, whereas the estimate derived for homogeneous media leads to an approximation of the time step 21% lower than the exact stability limit.

In the third case, the trace bound produces the best estimate of the stability limit, almost identical to the estimate obtained by the Irons and Treharne bound. It is also worth noting that the Brauer's bound produces accurate results. This example is used to emphasise that, based on the analysis described in Section C, it is not possible to discard any of the eigenvalue bounds considered. Despite the mean value of the error for the Brauer's bound is higher than the errors obtained with all the other bounds, as shown in Figure C1 , this particular example shows a situation where the Brauer's bound is able to outperform other eigenvalue bounds and provide an approximation of the stability limit very close to the ones provided by the Ostrowski's and trace bounds.

The fourth case illustrates a situation where the Irons and Treharne bound is less accurate. In this scenario, the accuracy of the stable time step provided by the use of any eigenvalue bounds is clearly limited by the accuracy of the Irons and Treharne bound. The best estimate of the stability limit is provided by the Ostrowski's bound. This estimate is 13% lower than the exact stability limit but only 6% lower than the Irons and Treharne bound. Finally, the estimate derived for homogeneous media leads to an approximation of the time step 40% lower than the exact stability limit and therefore resulting in a significant waste of computational resources.

The last case considered in Table 3 , shows an example where the estimate derived for homogeneous media leads to an unstable simulation, with an time step 8% higher than the stability limit. The best result is again provided by the Ostrowski's bound, only 7% below the exact stability limit and 3% below the bound derived from the Irons and Treharne theorem.

Table 4 shows the results for the realisations of the material parameters depicted in Figure 5 (b). The results show that

Case	Δt_{Ex}	Δt_{H}	Δt_{IT}	Δt_{F}	Δt_{P}	Δt_{O}	Δt_{B}	Δt_{T}
1	**0.000708**	0.000656	**0.000708**	0.000660	0.000579	0.000702	0.000669	**0.000707**
2	**0.000941**	0.000844	**0.000929**	0.000836	0.000783	**0.000905**	0.000689	0.000797
3	**0.001275**	**0.000842**	**0.001224**	0.001083	0.001063	**0.001180**	0.000944	0.001055
4	**0.000338**	**0.000184**	**0.000317**	0.000273	0.000272	0.000299	0.000282	**0.000303**
5	**0.000946**	**0.000971**	**0.000946**	0.000839	0.000765	**0.000922**	0.000792	0.000902

TABLE 4 Exact stability limit (Δt_{Ex}) compared to the estimate using the homogeneous material bound (Δt_{H}), the bound obtained by the theorem of Irons and Treharne (Δt_{IT}) and the bounds induced by the combination of the theorem of Irons and Treharne and the eigenvalue bounds presented in Section 5.1 for the realisations of the material parameters shown in Figure 5 (b).

the Ostrowski's and the trace bound always produce the best estimate of the exact stability limit. In the third and fourth cases in Table 4 , the estimate derived for homogeneous media leads to an approximation of the time step 34% and 46% lower than the exact stability limit and therefore resulting in a significant waste of computational resources, respectively. The last case in Table 4 shows again a scenario where the use of the estimate derived for homogeneous media leads to unstable results.

It is worth noting that the examples considered here correspond to a moderate value of the variance of the material properties and the correlation length, namely $\tilde{\sigma} = 1$ and $\ell = 2h$. When $\tilde{\sigma}$ is increased and/or ℓ decreased, numerical examples reveal that using the theoretical results derived for homogeneous media commonly lead to either very conservative estimates or overestimates of the exact stability limit. For instance, Table 5 shows the results for three cases generated with $\tilde{\sigma} = 1$ and $\ell = h/5$. In all cases, the best estimates obtained with the eigenvalue bound lead to time steps less than 1% lower than the bound provided by the Irons and Treharne theorem. In contrast, the time step computed from the homogeneous medium bound leads to either very conservative estimates or an overestimate of the stability time step. The realisations of the material parameters associated to the cases analysed in Table 5 are shown in Figure 6 (a).

Case	Δt_{Ex}	Δt_{H}	Δt_{IT}	Δt_{F}	Δt_{P}	Δt_{O}	Δt_{B}	Δt_{T}
1	**0.001113**	**0.000178**	**0.001076**	0.000917	0.000837	0.000971	0.000862	**0.001073**
2	**0.000851**	**0.000404**	**0.000740**	**0.000736**	0.000553	**0.000736**	0.000566	0.000734
3	**0.000496**	**0.000686**	**0.000470**	0.000431	0.000385	0.000431	0.000407	**0.000469**

TABLE 5 Exact stability limit (Δt_{Ex}) compared to the estimate using the homogeneous material bound (Δt_{H}), the bound obtained by the theorem of Irons and Treharne (Δt_{IT}) and the bounds induced by the combination of the theorem of Irons and Treharne and the eigenvalue bounds presented in Section 5.1 for the realisations of the material parameters shown in Figure 6 (a).

Table 6 shows the results for three realisations generated with $\tilde{\sigma} = 10$ and $\ell = 2h$, as shown in Figure 6 (b). In all cases the best estimates obtained with the eigenvalue bound lead to time steps less than 10% lower than the bound provided by the Irons and Treharne theorem. In contrast, the time step computed from the homogeneous medium bound lead to either very conservative estimates or an overestimate of the stability time step.

The last column in Table 6 shows the stiff-vertex stability limit derived in Section 4. It can be observed that the result always provides a conservative estimate of the exact stability limit. It is worth noting that in two of the three cases shown in Table 6 the stiff-vertex stability limit provides a very accurate estimate, almost as good as the best of the estimates provided by the eigenvalue bounds.

Finally, it is important to emphasize that the results obtained from the bound derived for homogeneous media are shown for illustration purposes only as, in practice, it is not possible to know a priori if the time step will result in an unstable simulation or a very conservative estimate.

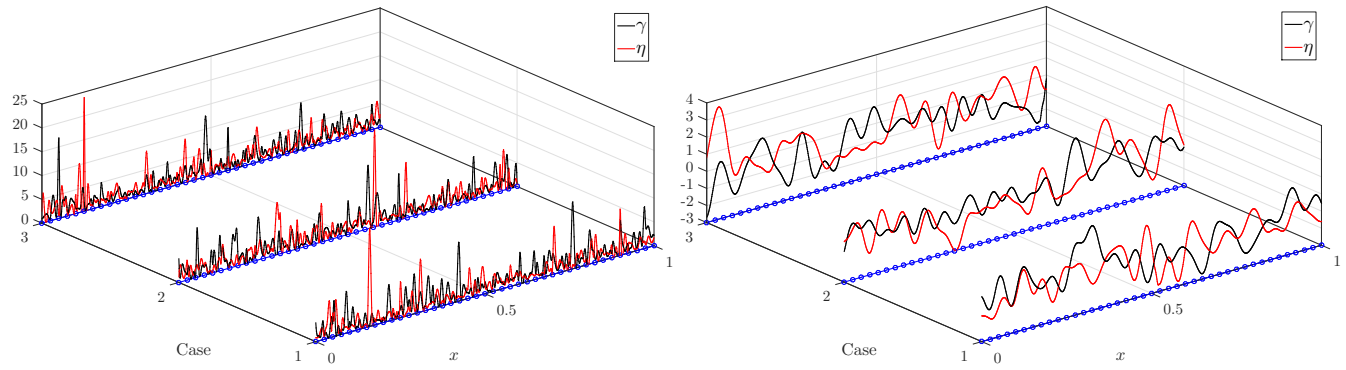

(a) $\tilde{\sigma} = 1$ and $\ell = h/5$ (b) $\tilde{\sigma} = 10$ and $\ell = 2h$

FIGURE 6 Realizations of the material parameters with $\mu = 2$ and $p = 5$. In (b) a logarithmic scale is used.

Case	Δt_{Ex}	Δt_{H}	Δt_{IT}	Δt_{F}	Δt_{P}	Δt_{O}	Δt_{B}	Δt_{T}	Δt_{SV}
1	**0.7794**	**0.2434**	**0.7445**	0.6288	0.6371	0.6411	0.6442	**0.6511**	0.4454
2	**0.4926**	0.4088	**0.4926**	0.4539	0.3678	0.4917	0.4775	**0.4926**	0.4903
3	**0.5987**	**1.0526**	**0.5259**	0.2093	0.1997	0.3847	0.2118	**0.5240**	0.4795

TABLE 6 Exact stability limit (Δt_{Ex}) compared to the estimate using the homogeneous material bound (Δt_{H}), the bound obtained by the theorem of Irons and Treharne (Δt_{IT}) and the bounds induced by the combination of the theorem of Irons and Treharne, the eigenvalue bounds presented in Section 5.1 and the stiff-vertex bound derived in Section 4, for the realisations of the material parameters shown in Figure 6 (b). All time steps have been multiplied by 10^4.

7.2 | Large scale simulation of wave propagation in a 3D randomly-heterogeneous medium

The use of the different stability criteria introduced in this paper is now illustrated with an example of practical interest. The wave propagation problem governed by Equation (2) is considered in a 3D heterogeneous medium with randomly-fluctuating parameters $\eta(\boldsymbol{x})$ and $\gamma(\boldsymbol{x})$. The domain is a cube of side $L = 20$ m, centred around $(0, 0, -10)$. Dirichlet boundary conditions are considered on all sides of the cube. The source is a Ricker impulse with central frequency $f_0 = 0.3$ Hz and time lag $\tau_0 = 3$ s centred at $(0, 5, -7)$. A receiver is placed at position $(6, -9, 0)$. The domain is meshed with $N^3 = 8\,000$ uniform hexahedra of side $L/N = 1$ m. Polynomials or order $p = 4$ are chosen in each direction, so that each element is discretised using $(4+1)^3 = 125$ degrees of freedom, for a total of 531 441 degrees of freedom. Simulations are run with different time steps, in order to localize precisely the transition to instability. The simulation durations range from a few seconds to a few minutes on 12 processors of an Intel Xeon E5-2670v3@2.30GHz node, depending on the particular realisation of the heterogeneous parameters and the chosen time step.

The parameters $\eta(\boldsymbol{x})$ and $\gamma(\boldsymbol{x})$ are modelled as independent Gaussian random fields with Gaussian correlation model, locally modified by Rosenblatt transform such that their first-order marginal density is log-normal with averages $\underline{\gamma} = 1$ N/m^2 and $\underline{\eta} = 2.67$ kg/m^3 and standard deviations $\sigma_\gamma = 5$ N/m^2 and $\sigma_\eta = 5$ N/m^2. Two different cases are considered with correlation length $\ell = 2h = 2$ m (shown in Figure 7) and $\ell = h/5 = 0.2$ m (shown in Figure 8).

For both cases with $\ell = 2h$ and $\ell = h/5$, a series of increasing time steps is considered and the value of the velocity in the receiver at time $t = 10$ s and $t = 16$ s is monitored. These instants correspond to the first wave arrival at the receiver. The lowest value of the time step for which the monitored velocity shoots up is a numerical estimation of the instability limit. Numerically, it is verified that this value is very close to the theoretical stability values reported in Table 7 , and obtained from the maximum eigenvalue of the dispersion matrix. This value is compared in Table 7 to the different bounds discussed in this paper. It appears clearly that all bounds are accurate, except the Brauer bound and the homogeneous bound. The latter in particular might induce a choice of time step 50% below the stability limit, while using the trace bound for instance would allow reaching 90% of that limit. It is worth noting that the stiff-vertex bound produces an accurate estimate in the second example, for which $\ell = h/5$.

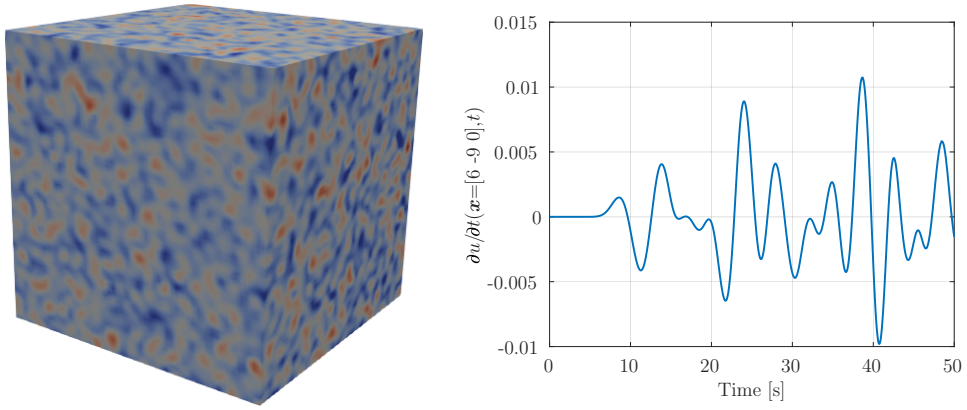

FIGURE 7 Map of density $\eta(\boldsymbol{x})$ in log-scale (left) and trace of the velocity in the receiver (right), for the large scale three-dimensional case with $\ell = 2h$. The simulation was performed with $\Delta t = 0.0434$ s.

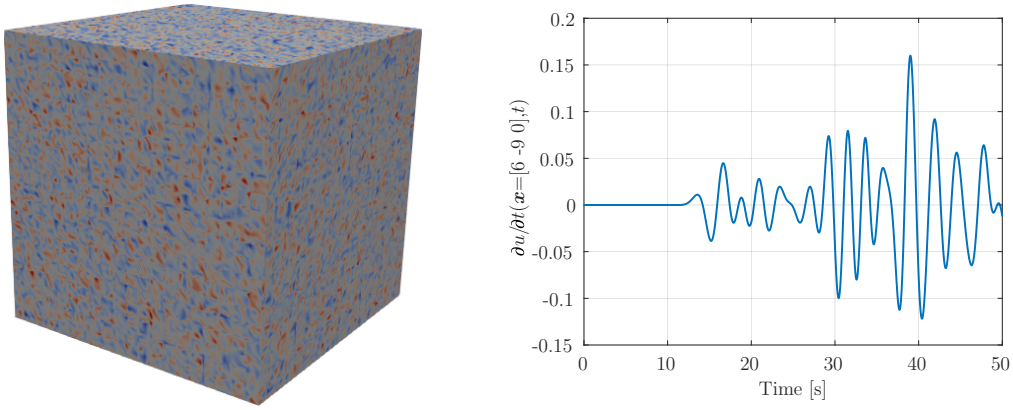

FIGURE 8 Map of density $\eta(\boldsymbol{x})$ in log-scale (left) and trace of the velocity in the receiver (right), for the large scale three-dimensional case with $\ell = h/5$. The simulation was performed with $\Delta t = 0.0511$ ms.

Case	$\Delta t_{\mathtt{Ex}}$	$\Delta t_{\mathtt{H}}$	$\Delta t_{\mathtt{IT}}$	$\Delta t_{\mathtt{F}}$	$\Delta t_{\mathtt{P}}$	$\Delta t_{\mathtt{0}}$	$\Delta t_{\mathtt{B}}$	$\Delta t_{\mathtt{T}}$	$\Delta t_{\mathtt{SV}}$
$\ell = 2h$	**0.14165**	**0.06701**	**0.14165**	0.14112	0.10466	0.14112	0.12727	**0.14114**	0.12034
$\ell = h/5$	**0.11212**	**0.07892**	**0.11150**	0.11128	0.07767	0.11128	0.10951	**0.11150**	0.11110

TABLE 7 Exact stability limit ($\Delta t_{\mathtt{Ex}}$) compared to the estimate using the homogeneous material bound ($\Delta t_{\mathtt{H}}$), the bound obtained by the theorem of Irons and Treharne ($\Delta t_{\mathtt{IT}}$) and the bounds induced by the combination of the theorem of Irons and Treharne, the eigenvalue bounds presented in Section 5.1 and the stiff-vertex bound derived in Section 4, for the large scale 3D cases. Times are in ms.

8 | CONCLUSION

The stability of an explicit Leap-Frog time marching scheme for the simulation of wave propagation in randomly-heterogeneous media with high-order spectral elements has been considered. By using the so-called Irons and Treharne theorem, the global stability criterion is taken as a minimum over local element stability criteria, obtained through the solution of element-borne eigenvalue problems.This work proposes two alternatives to estimate the maximum eigenvalue of the elemental dispersion matrix, avoiding the computation of the exact maximum eigenvalue, which is considered a not viable option for high-order elements due to the size of the elemental matrices in this context.

The first type of stability criterion was obtained in the particular setting of strongly-heterogeneous rapidly-fluctuating media through asymptotic analysis. This criterion depends only on the maximum velocity at the vertices of the mesh, and not on the velocity at the interior nodes. More particularly, it shows that stability is improved if the large values of the local velocities are found at the interior nodes of the elements rather than on their boundaries. This is consistent with results obtained in [18], in a very different setting (periodically-fluctuating quadratic spectral elements). It might provide leads to improve stability through mesh distortion, although the impact of that mesh distortion on stability would also have to be evaluated.

For more general situations, different bounds on the eigenvalues of general matrices were recalled to approximate the global stability criterion conservatively. The accuracy of the proposed stability limits have been tested with an extensive set of experiments in one, two and three dimensions. For all cases tested, the Trace and Ostrowski bounds seemed to provide particularly accurate estimates of the actual stability criteria. The numerical examples involving the wave propagation in randomly-heterogeneous media in two and three dimensions corroborate the findings and provide a clear illustration of the problems induced by the extended approach of adapting the stability limit derived for homogeneous media to a heterogeneous media.

As a conclusion, it should be reminded that this paper focused on the acoustic case for the SEM with Gauss-Lobatto-Legendre points and the Leap-Frog time integration scheme. However, the ideas proposed are general and can be directly applied to study the stability of other formulations of the SEM [25,26] and other time integrators [27,28], for both acoustic or elastic equations.

□

APPENDIX

A STABILITY OF STRONGLY-HETEROGENEOUS RAPIDLY-FLUCTUATING RANDOM MEDIA

In this Appendix, the proof of Proposition 1 of Section 4. This proof is based on the following lemmas:

Lemma 1. Let us consider $\mathbf{a}$ a vector in a basis of dimension N, $\mathbf{e}$ be one of the elements of that basis, and $\mathbf{B}$ be an $N \times N$ square matrix in the same basis. If all vectors and matrices are real and their norm is of order $\mathcal{O}(1)$, then

$$\det\left(\mathbf{e}\otimes\mathbf{a}-\lambda\mathbf{I}_N+\epsilon\mathbf{B}\right)=-(-\lambda)^{N-2}\left\{\lambda^2-\lambda\left[\mathbf{a}\cdot\mathbf{e}+\epsilon\mathrm{tr}(\mathbf{B})\right]-\epsilon\mathbf{a}\cdot\left[\mathbf{B}-\mathrm{tr}(\mathbf{B})\mathbf{I}_N\right]\mathbf{e}\right\}+o(\epsilon), \tag{A1}$$

for all $\lambda \in \mathbb{R}$, where $\mathbf{I}_N$ is the $N \times N$ identity matrix.

Proof. The Taylor expansion of the determinant of a matrix to first order in ϵ yields

$$\det\left(\mathbf{e}\otimes\mathbf{a}-\lambda\mathbf{I}_N+\epsilon\mathbf{B}\right)=\det\left(\mathbf{e}\otimes\mathbf{a}-\lambda\mathbf{I}_N\right)\left\{1+\epsilon\mathrm{tr}\left(\left[\mathbf{e}\otimes\mathbf{a}-\lambda\mathbf{I}_N\right]^{-1}\mathbf{B}\right)\right\}+o(\epsilon) \tag{A2}$$

Using Sherman-Morrison formula, we have that

$$\left(\mathbf{e}\otimes\mathbf{a}-\lambda\mathbf{I}_N\right)^{-1}=-\frac{1}{\lambda}\left(\mathbf{I}_N+\frac{\mathbf{e}\otimes\mathbf{a}}{\lambda-\mathbf{a}\cdot\mathbf{e}}\right), \tag{A3}$$

which implies

$$\mathrm{tr}\left(\left[\mathbf{e}\otimes\mathbf{a}-\lambda\mathbf{I}_N\right]^{-1}\mathbf{B}\right)=-\frac{1}{\lambda}\left(\mathrm{tr}(\mathbf{B})+\frac{\mathbf{a}\cdot\mathbf{B}\cdot\mathbf{e}}{\lambda-\mathbf{a}\cdot\mathbf{e}}\right). \tag{A4}$$

Combining the fact that $\det\left(\mathbf{e}\otimes\mathbf{a}-\lambda\mathbf{I}_N\right)=(\mathbf{a}\cdot\mathbf{e}-\lambda)(-\lambda)^{N-1}$ and Equation (A4) in Equation (A2), the expected expansion is obtained. □

Lemma 2. With the same hypothesis of Lemma 1, the maximum eigenvalue of $\mathbf{e}\otimes\mathbf{a}+\epsilon\mathbf{B}$ is equal to

$$\lambda_{\max}=\mathbf{a}\cdot\mathbf{e}+\epsilon\frac{\mathbf{a}\cdot\mathbf{B}\cdot\mathbf{e}}{\mathbf{a}\cdot\mathbf{e}}+o(\epsilon). \tag{A5}$$

Proof. Using Lemma 1, the three eigenvalues are, asymptotically, 0, with multiplicity $N-2$, $\epsilon[\mathrm{tr}(\mathbf{B})-(\mathbf{a}\cdot\mathbf{B}\cdot\mathbf{e})]/(\mathbf{a}\cdot\mathbf{e})+o(\epsilon)$ and the eigenvalue in Equation A5. Being the only eigenvalue of order $\mathcal{O}(1)$, and with a positive leading-order coefficient, the latter eigenvalue is the maximum. □

Using Lemmas 1 and 2, the proof of Proposition 1 is now provided.

Proof. The one-dimensional case is considered first. It is assumed that the n-th element node has a low value of the density and a large value of the stiffness. For the reasons exposed in Section 4, the studiy is limited to the case where the node corresponds to an element vertex, *i.e.* $n = 1$ (the situation with $n = \mathtt{n}_{\mathtt{en}}$ is equivalent).

It is worth noting that the scaled elemental dispersion matrix, $\epsilon^2\mathbf{D}^e$, can be written in the form of Lemma 2 with

$$a_j = \epsilon^2 \left(\frac{2}{h}\right)^2 \frac{\gamma_1^e}{\eta_1^e} d_{11} d_{j1}, \quad B_{1j} = \epsilon \left(\frac{2}{h}\right)^2 \sum_{k=2}^{\mathtt{n}_{\mathtt{en}}} \frac{\gamma_k^e \omega_k}{\eta_1^e \omega_1} d_{1k} d_{jk}, \quad B_{i>1j} = \epsilon \left(\frac{2}{h}\right)^2 \frac{\gamma_1^e \omega_1}{\eta_i^e \omega_i} d_{i1} d_{j1}, \tag{A6}$$

and with higher order terms in ϵ that do not play a role in this analysis. Using Lemma 2, the maximum eigenvalue is then

$$\lambda_{\max} = \left(\frac{2}{h}\right)^2 \left(\frac{\gamma_1^e}{\eta_1^e} d_{11}^2 + \sum_{k=2}^{\mathtt{n}_{\mathtt{en}}} \frac{\gamma_k^e \omega_k}{\eta_1^e \omega_1} d_{1k}^2 + \sum_{k=2}^{\mathtt{n}_{\mathtt{en}}} \frac{\gamma_1^e \omega_1}{\eta_k^e \omega_k} d_{k1}^2 \right) + \mathcal{O}\left(\epsilon^{-1}\right) = \mathrm{tr}(\mathbf{D}^e) + \mathcal{O}\left(\epsilon^{-1}\right). \tag{A7}$$

This result extends naturally to higher dimensions by simply replacing the term d_{ij} by the appropriate derivative.

Finally, to prove that this value is actually an upper bound, it is sufficient to recall that the trace of a matrix is equal to the sum of the eigenvalues of the matrix and that the eigenvalues of a dispersion matrix are all positive. The latter result can be obtained with a lower bound[49] on the smallest eigenvalue of the dispersion matrix, which is positive when the matrix is a product of a definite positive matrix (the inverse of the mass matrix) and a positive matrix (the stiffness matrix). Then is is clear that

$$\lambda_{\max} \leq \mathrm{tr}(\mathbf{D}^e). \tag{A8}$$

□

B OPTIMALITY OF THE EIGENVALUE BOUNDS FOR LINEAR SPECTRAL ELEMENTS IN ONE DIMENSION

As a first measure of the accuracy of the eigenvalue bounds summarised in Section 5.1, their optimality for the simplest case in a heterogeneous medium is considered. For linear one-dimensional elements (i.e. $p = 1$) with heterogeneous material properties, the elemental mass and stiffness matrices are

$$\mathbf{M}^e = \frac{h}{2} \begin{pmatrix} \eta_1 & 0 \\ 0 & \eta_2 \end{pmatrix}, \qquad \mathbf{K}^e = \frac{(\gamma_1 + \gamma_2)}{2h} \begin{pmatrix} 1 & -1 \\ -1 & 1 \end{pmatrix}. \tag{B9}$$

The dispersion matrix, given by

$$\mathbf{D}^e = \frac{(\gamma_1 + \gamma_2)}{\eta_1 \eta_2 h^2} \begin{pmatrix} \eta_2 & -\eta_2 \\ -\eta_1 & \eta_1 \end{pmatrix}, \tag{B10}$$

has maximum eigenvalue

$$\lambda_{\max}^e = \frac{1}{h^2}(\gamma_1 + \gamma_2) \left(\frac{1}{\eta_1} + \frac{1}{\eta_2} \right). \tag{B11}$$

B.1 Frobenius' bound

The Frobenius' bound of Equation 26 for linear elements in one dimension gives

$$\lambda_{\mathtt{F}}(\mathbf{D}^e) = \frac{1}{h^2}(\gamma_1 + \gamma_2) \frac{1}{\eta_1 \eta_2} \min\left\{ 2 \max\left\{ \eta_1, \eta_2 \right\}, \eta_1 + \eta_2 \right\}, \tag{B12}$$

which is equal to the eigenvalue in Equation (B11) and therefore, optimal.

B.2 Parkers' bound

For linear elements in one dimension, the Parker's bound of Equation 31 gives

$$\lambda_{\mathtt{P}}(\mathbf{D}^e) = \frac{1}{2h^2}(\gamma_1 + \gamma_2) \frac{1}{\eta_1 \eta_2} \left(2 \max\left\{ \eta_1, \eta_2 \right\} + \eta_1 + \eta_2 \right). \tag{B13}$$

After some basic manipulations, it can be shown that

$$\lambda_{\mathtt{P}}(\mathbf{D}^e) = \frac{1}{2} \lambda_{\mathtt{LHG}}(\mathbf{D}^e) + \frac{1}{2} \lambda_{\max}^e. \tag{B14}$$

Therefore, as the the Lévy-Hadamard-Gerschgorin bound, the Parker's bound is only optimal when $\eta_1 = \eta_2$.

B.3 Ostrowski's bound

The computation of the terms in Equation (32) for linear elements in one dimension leads to the following expression for the Ostrowski's bound

$$\lambda_0(\mathbf{D}^e) = \frac{1}{h^2}(\gamma_1+\gamma_2)\frac{1}{\eta_1\eta_2}\max\left\{\eta_1+\min\{\eta_1,\eta_2\},\eta_2+\min\{\eta_1,\eta_2\}\right\}. \tag{B15}$$

which, after some manipulations, can be shown to be optimal.

B.4 Brauer's bound

For linear elements in one dimension, the Brauer's bound of Equation 33 gives

$$\lambda_{\text{B}}(\mathbf{D}^e) = \frac{1}{2h^2}(\gamma_1+\gamma_2)\frac{1}{\eta_1\eta_2}\left(\eta_1+\eta_2+\sqrt{(\eta_1-\eta_2)^2+4\eta_1\eta_2}\right). \tag{B16}$$

After some basic manipulations, it is easy to show that is optimal.

B.5 Trace bound

A simple calculation of the terms in Equation (35) for linear elements in one dimension shows that the maximum eigenvalue coincides with the trace bound because

$$\bar{\lambda}(\mathbf{D}^e) = \sigma(\mathbf{D}^e) = \frac{1}{2h^2}(\gamma_1+\gamma_2)\left(\frac{1}{\eta_1}+\frac{1}{\eta_2}\right). \tag{B17}$$

C SHARPNESS OF THE EIGENVALUE BOUNDS

To illustrate the sharpness of the eigenvalue bounds considered in this work, Figure C1 shows the mean value of the relative difference, in logarithmic scale, between the maximum eigenvalue of an one-dimensional elemental dispersion matrix and the bounds presented in Section 5.1. The mechanical parameters γ and η at the nodes are modelled as realisations of log-normal random variables with average $\mu = 2$, variance $\sigma^2 = (\tilde{\sigma}\mu)^2$, where $\tilde{\sigma} \in [0.01, 10]$, and correlation length $\ell = 2h$, where h is the characteristic element size. The results show the mean value of $\epsilon_{\texttt{Bound}}$ for a degree of approximation p ranging from 1 to 8 on a one-dimensional element and by using 10,000 realisations of the mechanical properties.

For linear elements (i.e. $p = 1$) the Frobenius', Ostrowski's, Brauer's and trace bounds are optimal, as shown in Section 5.1. For higher order elements the different bounds show a different behaviour.

The difference between the Frobenius' bound and the exact eigenvalue shows a very small dependence on both the degree of the approximation, p, and the variance of the material properties, $\tilde{\sigma}$. Only for quadratic elements (i.e. $p = 2$) and for a high value of $\tilde{\sigma}$, the Frobenius' bound provides a less accurate estimate of the maximum eigenvalue. Similarly, the Ostrowski's bound shows almost no dependence on the degree of approximation and the variance of the material properties. For quadratic elements and a low value of $\tilde{\sigma}$ the Ostrowski's bound provides more accurate results. The other bounds, namely the Parker's, Brauer's and trace bounds, show a sizeable dependence on both p and $\tilde{\sigma}$.

Overall, it is apparent that the Ostrowski's bound and the trace bound provide the sharpest estimate of the maximum eigenvalue for the values of p and $\tilde{\sigma}$ considered, whereas the Brauer's bound provide the less accurate results.

A similar study is also performed in two dimensions. Figure C2 shows the mean value of the relative difference, in logarithmic scale, between the maximum eigenvalue of a two-dimensional elemental dispersion matrix and the bounds presented in Section 5.1. As in the previous example, the mechanical parameters γ and η at the nodes are modelled as realisations of log-normal random variables with average $\mu = 2$ and variance $\sigma^2 = (\tilde{\sigma}\mu)^2$, where $\tilde{\sigma} \in [0.01, 10]$. The results show the mean value of $\epsilon_{\texttt{Bound}}$ for a degree of approximation p ranging from 1 to 8 on a one-dimensional element and by using 10,000 realisations of the mechanical properties.

Important differences are observed between the accuracy provided by some bounds in one and two dimensions. The Frobenius' bound provide significantly better results in two dimensions and, as in the one-dimensional example, the sharpness of the estimate produced shows a very small dependence on the degree of approximation, p, and the variance of the material properties, $\tilde{\sigma}$. The Parker's bound provides better results in two dimensions for particular cases with $p = 1$ and a high value of $\tilde{\sigma}$, but, overall, the performance is very similar in one and two dimensions. The Ostrowski's bound also shows a very similar behaviour for both one

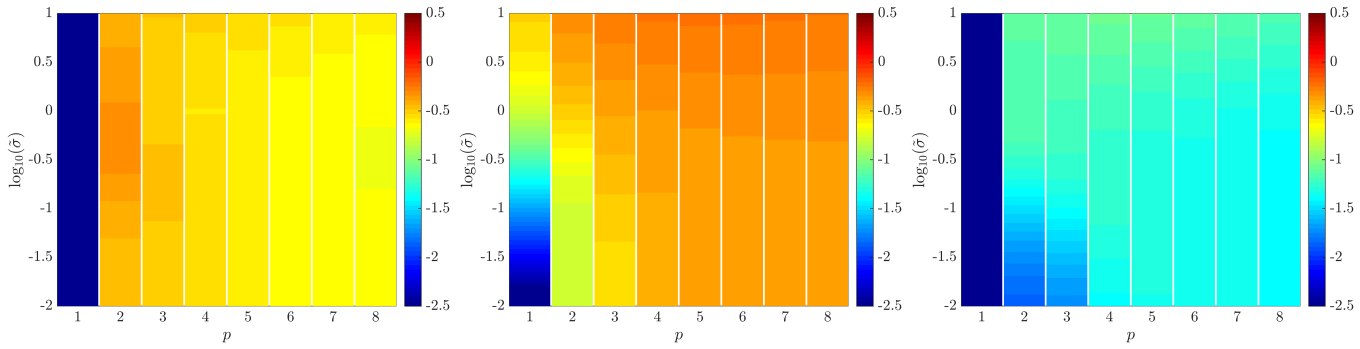

(a) Frobenius' bound (b) Parker's bound (c) Ostrowski's bound

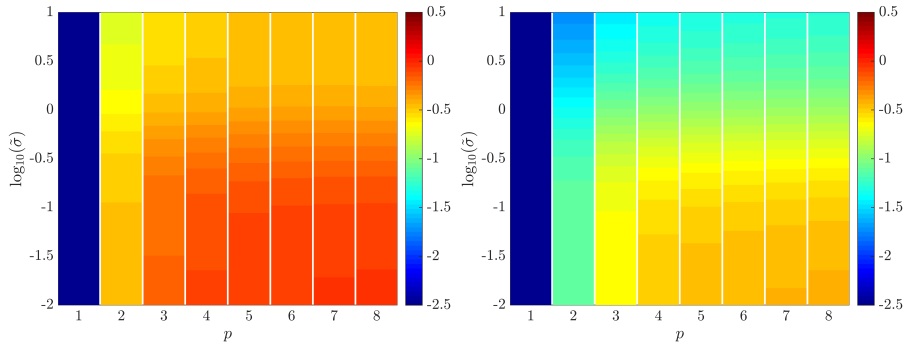

(d) Brauer's bound (e) Trace bound

FIGURE C1 Mean value of the relative difference between the maximum eigenvalue of the one-dimensional elemental dispersion matrix and the eigenvalues bounds of Section 5.1 in logarithmic scale. The mechanical parameters are modelled as 10,000 realisations of log-normal random variables with average $\mu = 2$, variance $\sigma^2 = (\tilde{\sigma}\mu)^2$ and correlation length $\ell = 2h$.

and two-dimensional problems. It is interesting to observe that, for low values of $\tilde{\sigma}$, the Ostrowski's bound seems to provide better results for two-dimensional problems. The Brauer's bound shows a very similar behaviour for one and two-dimensional problems with a slight low accuracy in two dimensions. Finally, the trace bound shows the most sizeable deterioration in two-dimensional problems compared to the results for obtained in one dimension.

Overall, the results show that the the Frobenius' and the Ostrowski's bound provide the sharpest estimate of the maximum eigenvalue for the values of p and $\tilde{\sigma}$ considered, whereas the Brauer's bound provide the less accurate results.

For completeness, the same study is performed in three dimensions next. Figure C3 shows the mean value of the relative difference, in logarithmic scale, between the maximum eigenvalue of a two-dimensional elemental dispersion matrix and the bounds presented in Section 5.1. As in the previous example, the mechanical parameters γ and η at the nodes are modelled as realisations of log-normal random variables with average $\mu = 2$ and variance $\sigma^2 = (\tilde{\sigma}\mu)^2$, where $\tilde{\sigma} \in [0.01, 10]$. The results show the mean value of $\epsilon_{\texttt{Bound}}$ for a degree of approximation p ranging from 1 to 8 on a one-dimensional element and by using 10,000 realisations of the mechanical properties. In this case, the behaviour is very similar to the two-dimensional case, with a slight deterioration on the accuracy obtained by all the proposed bounds. It is interesting to observe that even for linear elements with a large value of the variance of the material properties, $\tilde{\sigma}$, the results a sizeable deterioration with respect to the two-dimensional case is observed. Similarly to the two-dimensional example, the results show that the the Frobenius' and the Ostrowski's bound provide the sharpest estimate of the maximum eigenvalue for the values of p and $\tilde{\sigma}$ considered.

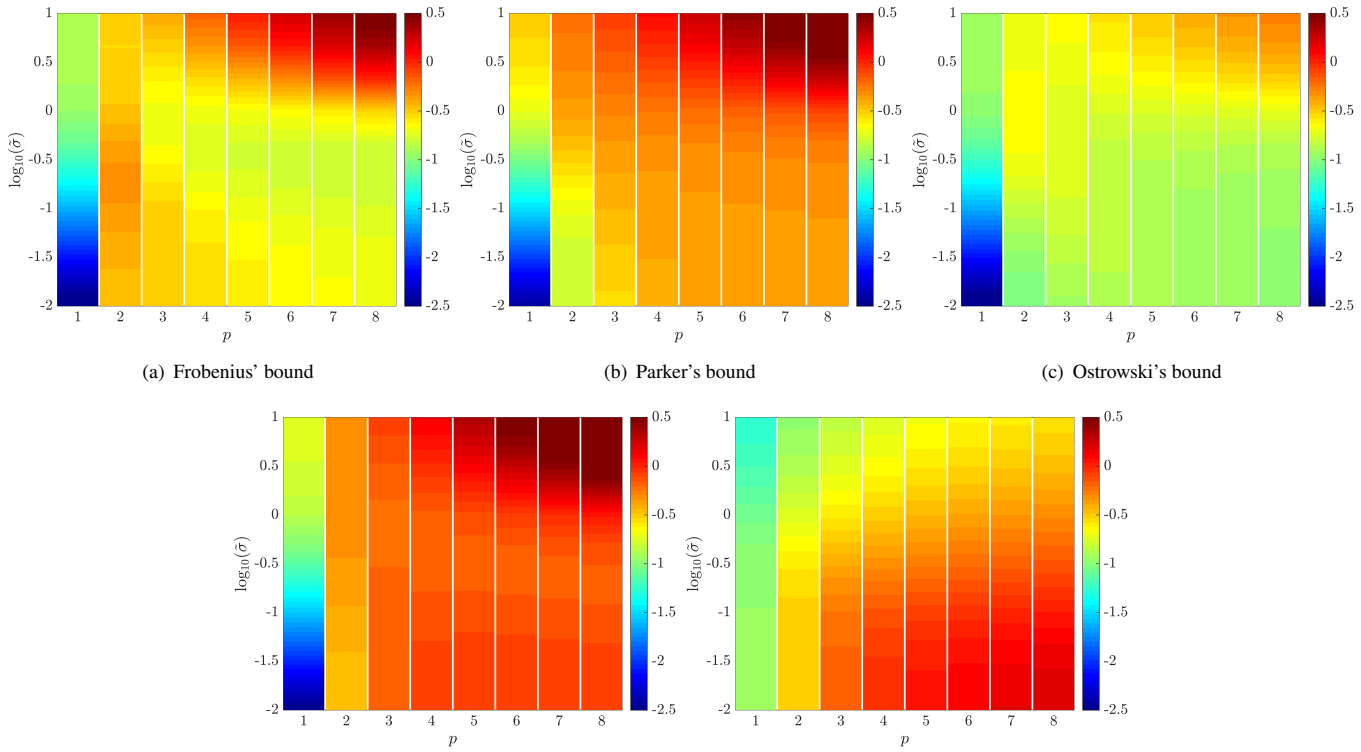

(a) Frobenius' bound (b) Parker's bound (c) Ostrowski's bound

(d) Brauer's bound (e) Trace bound

FIGURE C2 Mean value of the relative difference between the maximum eigenvalue of the two-dimensional elemental dispersion matrix and the eigenvalues bounds of Section 5.1 in logarithmic scale. The mechanical parameters are modelled as 10,000 realisations of log-normal random variables with average $\mu = 2$, variance $\sigma^2 = (\tilde{\sigma}\mu)^2$ and correlation length $\ell = 2h$.

ACKNOWLEDGEMENTS

The spectral element software used for the simulation in the last part of this paper is developed jointly by CentraleSupélec, CEA Commissariat à l'Énergie Atomique and Institut de Physique du Globe de Paris. Within the SINAPS@ project, this development benefited from French state funding managed by the National Research Agency under program RNSR Future Investments bearing reference No. ANR-11-RSNR-0022-04. This work was performed using HPC resources from the "Mésocentre" computing center of CentraleSupélec and École Normale Supérieure Paris-Saclay, supported by CNRS and the French Ministère de l'Enseignement Supérieur, de la Recherche, et de l'Innovation (http://mesocentre.centralesupelec.fr/).

References

1. Komatitsch D., Tsuboi S., Tromp J.. The spectral-element method in seismology. In: Levander A., Nolet G., eds. *Seismic Earth: Array Analysis of Broadband Seismograms*, Geophysical Monograph, vol. 157: :205-228American Geophysical Union; 2005.

2. Sun Jia-Hong, Wu Tsung-Tsong. Propagation of acoustic waves in phononic-crystal plates and waveguides using a finite-difference time-domain method. *Physical Review B.* 2007;76(10):104304.

3. Christodoulou K, Laghrouche O, Mohamed MS, Trevelyan J. High-order finite elements for the solution of Helmholtz problems. *Computers & Structures.* 2017;191:129–139.

4. Dawson Mark, Sevilla Ruben, Morgan Kenneth. The application of a high-order discontinuous Galerkin time-domain method for the computation of electromagnetic resonant modes. *Applied Mathematical Modelling.* 2018;55:94–108.

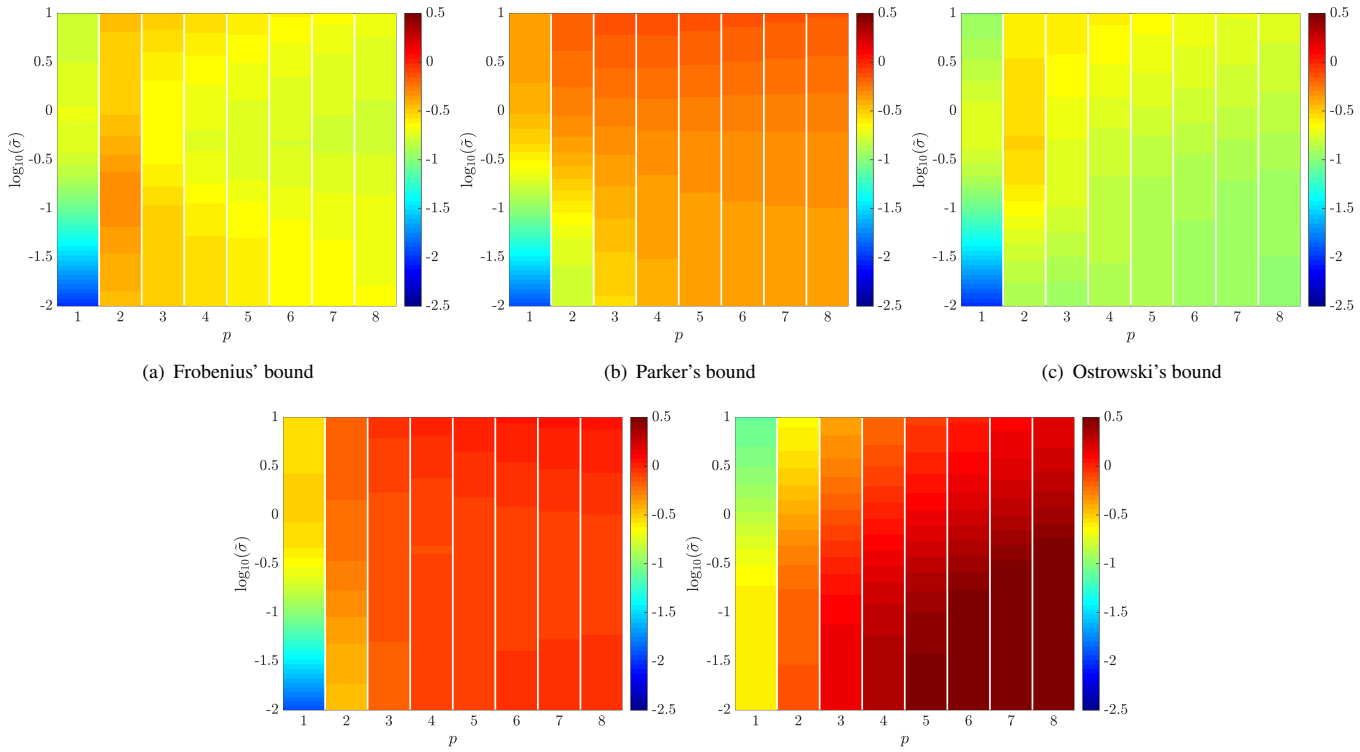

(a) Frobenius' bound (b) Parker's bound (c) Ostrowski's bound

(d) Brauer's bound (e) Trace bound

FIGURE C3 Mean value of the relative difference between the maximum eigenvalue of the three-dimensional elemental dispersion matrix and the eigenvalues bounds of Section 5.1 in logarithmic scale. The mechanical parameters are modelled as 10,000 realisations of log-normal random variables with average $\mu = 2$, variance $\sigma^2 = (\tilde{\sigma}\mu)^2$ and correlation length $\ell = 2h$.

5. Cohen G. *Higher-order numerical methods for transient wave equations*. Springer; 2001.

6. De Basabe J. D., Sen M. K.. Grid dispersion and stability criteria of some common finite-element methods for acoustic and elastic wave equations. *Geophysics.* 2007;72(6):T81-T95.

7. De Basabe J. D., Sen M. K.. Stability of the high-order finite elements for acoustic or elastic wave propagation with high-order time stepping. *Geophysical Journal International.* 2010;181:577-590.

8. Agut Cyril, Diaz Julien. Stability analysis of the Interior Penalty Discontinuous Galerkin method for the wave equation. *ESAIM: Mathematical Modelling and Numerical Analysis.* 2013;47(3):903–932.

9. Mulder WA, Zhebel E, Minisini S. Time-stepping stability of continuous and discontinuous finite-element methods for 3-D wave propagation. *Geophysical Journal International.* 2014;196(2):1123–1133.

10. Seriani G, Oliveira SP. Dispersion analysis of spectral element methods for elastic wave propagation. *Wave Motion.* 2008;45(6):729–744.

11. Oliveira SP, Seriani G. Effect of element distortion on the numerical dispersion of spectral element methods. *Communications in Computational Physics.* 2011;9(4):937–958.

12. Zhu Liyong, Du Qiang. Mesh dependent stability and condition number estimates for finite element approximations of parabolic problems. *Mathematics of Computation.* 2014;83(285):37–64.

13. Askes H., Rodríguez-Ferran A., Hetherington J.. The effects of element shape on the critical time step in explicit time integrators for elasto-dynamics. *International Journal for Numerical Methods in Engineering.* 2015;101:809-824.

14. Shubin G. R., Bell J. B.. A modified equation approach to constructing fourth order methods for acoustic wave propagation. *SIAM Journal on Scientific and Statistical Computing.* 1987;8(2):135-151.

15. Maday Yvon, Rønquist Einar M. Optimal error analysis of spectral methods with emphasis on non-constant coefficients and deformed geometries. *Computer Methods in Applied Mechanics and Engineering.* 1990;80(1-3):91–115.

16. Seriani G., Priolo E.. Spectral element method for acoustic wave simulation in heterogeneous media. *Finite elements in analysis and design.* 1994;16(3):337-348.

17. Cohen G., Joly P.. Construction analysis of fourth-order finite difference schemes for the acoustic wave equation in nonhomogeneous media. *SIAM Journal on Numerical Analysis.* 1996;33(4):1266-1302.

18. Sevilla R., Cottereau R.. Influence of periodically fluctuating material parameters on the stability of explicit high order spectral element methods. *Journal of Computational Physics.* 2018;. Submitted for publication.

19. Ta Q.-A., Clouteau D., Cottereau R.. Modeling of random anisotropic elastic media and impact on wave propagation. *European Journal of Computational Mechanics.* 2010;19(1-3):241-253.

20. Jehel P., Cottereau R.. On damping created by heterogeneous yielding in the numerical analysis of nonlinear RC frame elements. *Computers & Structures.* 2015;154:192-203.

21. Khazaie S., Cottereau R., Clouteau D.. Numerical observation of the equipartition regime in a 3D randomly heterogeneous elastic medium, and discussion on the limiting parameters. *Computers & Geosciences.* 2017;102:56-67.

22. Svay A., Perron V., Imtiaz A., et al. Spatial coherency analysis of seismic ground motions from a rock site dense array implemented during the Kefalonia 2014 aftershock sequence. *Earthquake Engineering & Structural Dynamics.* 2017;46(12):1895-1917.

23. de Abreu Corrêa L., Quezada J. C., Cottereau R., Costa d'Aguiar S., Voivret C.. Randomly-fluctuating heterogeneous continuum model of a granular medium. *Computational Mechanics.* 2017;60(5):845-861.

24. Wathen A. J.. An analysis of some element-by-element techniques. *Computer Methods in Applied Mechanics and Engineering.* 1989;74:271-287.

25. Cohen G., Fauqueux S.. Mixed finite elements with mass-lumping for the transient wave equation. *J. Comput. Acoustics.* 2000;8(1):171-188.

26. Seriani G., Oliveira S. P.. Dispersion analysis of spectral element methods for elastic wave propagation. *Wave Motion.* 2008;45(6):729-744.

27. Nissen-Meyer T., Fournier A., Dahlen F. A.. A 2-D spectral-element method for computing spherical-earth seismograms – II. waves in solid-fluid media. *Geophys. J. Int..* 2008;174(3):873-888.

28. Xie Z., Komatitsch D., Martin R., Matzen R.. Improved forward wave propagation and adjoint-based sensitivity kernel calculations using a numerically stable finite-element PML. *Geophys. J. Int..* 2014;198:1714-1747.

29. Komatitsch D., Vilotte J.-P., Vai R., Castillo-Covarrubias J. M., Sánchez-Sesma F. J.. The spectral element method for elastic wave equations – application to 2-D and 3-D seismic problems. *International Journal for Numerical Methods in Engineering.* 1999;45(9):1139-1164.

30. Komatitsch Dimitri, Ritsema Jeroen, Tromp Jeroen. The spectral-element method, Beowulf computing, and global seismology.. *Science.* 2002;298(5599):1737-1742.

31. Cupillard P., Delavaud E., Burgos G., et al. RegSEM: a versatile code based on the spectral element method to compute seismic wave propagation at the regional scale. *Geophysical Journal International.* 2012;188(3):1203-1220.

32. Mazzieri I., Stupazzini M., Guidotti R., Smerzini C.. SPEED: SPectral Elements in Elastodynamics with Discontinuous Galerkin: a non-conforming approach for 3D multi-scale problems. *International Journal for Numerical Methods in Engineering.* 2013;95(12):991-1010.

33. Patera Anthony T. A spectral element method for fluid dynamics: laminar flow in a channel expansion. *Journal of Computational Physics.* 1984;54(3):468–488.

34. Karniadakis George, Sherwin Spencer. *Spectral/hp element methods for computational fluid dynamics*. Oxford University Press; 2013.

35. Funaro Daniele. *Polynomial approximation of differential equations*. Springer Science & Business Media; 2008.

36. Fried I. Bounds on the extremal eigenvalues of the finite element stiffness and mass matrices and their spectral condition number. *Journal of sound and vibration.* 1972;22(4):407–418.

37. Lin J. I.. An element eigenvalue theorem and its application for stable time steps. *Computer Methods in Applied Mechanics and Engineering.* 1989;73:283-294.

38. Fung TC. A precise time-step integration method by step-response and impulsive-response matrices for dynamic problems. *International Journal for Numerical Methods in Engineering.* 1997;40(24):4501–4527.

39. Telles JCF, Brebbia CA. Elastic/viscoplastic problems using boundary elements. *International Journal of Mechanical Sciences.* 1982;24(10):605–618.

40. Bueche D, Sukumar N, Moran B. Dispersive properties of the natural element method. *Computational Mechanics.* 2000;25(2):207–219.

41. Marcus Marvin, Minc Henryk. *A survey of matrix theory and matrix inequalities*. Courier Corporation; 1992.

42. Bodewig Ewald. *Matrix calculus*. Elsevier; 2014.

43. Schaeuble Anne-Kathrin, Tkachuk Anton, Bischoff Manfred. Time step estimates for explicit dynamics with reciprocal mass matrices. *Computers & Structures.* 2018;202:74–84.

44. Brauer Alfred, others . Limits for the characteristic roots of a matrix. *Duke Mathematical Journal.* 1946;13(3):387–395.

45. Wolkowicz Henry, Styan George PH. Bounds for eigenvalues using traces. *Linear algebra and its applications.* 1980;29:471–506.

46. Graybill Franklin A. *Matrices with applications in statistics*. Wadsworth Inc.; 1983.

47. LeVeque Randall J. Wave propagation algorithms for multidimensional hyperbolic systems. *Journal of Computational Physics.* 1997;131(2):327–353.

48. Fezoui Loula, Lanteri Stéphane, Lohrengel Stéphanie, Piperno Serge. Convergence and stability of a discontinuous Galerkin time-domain method for the 3D heterogeneous Maxwell equations on unstructured meshes. *ESAIM: Mathematical Modelling and Numerical Analysis.* 2005;39(6):1149–1176.

49. Mirsky L.. On the trace of matrix products. *Mathematische Nachrichten.* 1959;20(3-6):171-174.